

Deleted: measurement

*Correspondence to: hashim.al.hashimi@duke.edu

Abstract. In duplex DNA, Watson-Crick A-T and G-C base pairs (bps) exist in dynamic equilibrium with an alternative Hoogsteen conformation, which is low in abundance and short-lived. Measuring how the Hoogsteen dynamics varies across different DNA sequences, structural contexts and physiological conditions is key for identifying potential Hoogsteen hot spots and for understanding the potential roles of Hoogsteen base pairs in DNA recognition and repair. However, such studies are hampered by the need to prepare ^{13}C or ^{15}N isotopically enriched DNA samples for NMR relaxation dispersion (RD) experiments. Here, using SElective Optimized Proton Experiments (SELOPE) ^1H CEST experiments employing high-power radiofrequency fields ($B_1 > 250$ Hz) targeting imino protons, we demonstrate accurate and robust characterization of Watson-Crick to Hoogsteen exchange, without the need for isotopic enrichment of the DNA. For 13 residues in three DNA duplexes under different temperature and pH conditions, the exchange parameters deduced from high-power imino ^1H CEST were in very good agreement with counterparts measured using off-resonance $^{13}\text{C}/^{15}\text{N}$ spin relaxation in the rotating frame ($R_{1\rho}$). It is shown that ^1H - ^1H NOE effects which typically introduce artifacts in ^1H based measurements of chemical exchange can be effectively suppressed by selective excitation, provided that the relaxation delay is short (≤ 100 ms). The ^1H CEST experiment can be performed with $\sim 10\text{X}$ higher throughput and $\sim 100\text{X}$ lower cost relative to $^{13}\text{C}/^{15}\text{N}$ $R_{1\rho}$, and enabled Hoogsteen

Deleted: understanding

Deleted: the role of these non-canonical bps in

34 chemical exchange measurements undetectable by $R_{1\rho}$. The results reveal an
35 increased propensity to form Hoogsteen bps near terminal ends and a diminished
36 propensity within A-tract motifs. The ^1H CEST experiment provides a basis for
37 rapidly screening Hoogsteen breathing in duplex DNA, enabling identification of
38 unusual motifs for more in-depth characterization.

Deleted: opens

Deleted: the door to more comprehensively
characterizing ...

1 Introduction

Soon after the discovery of the DNA double helix, it was shown that A-T and G-C could also pair in an alternative conformation known as the “Hoogsteen” base pair (bp) (Felsenfeld et al., 1957; Hoogsteen, 1959) (Fig. 1a). Starting from a canonical Watson-Crick G-C or A-T bp, the corresponding Hoogsteen bp can be obtained by flipping the purine base 180° and bringing the two bases into proximity to create a new set of hydrogen-bonds, which in the case of G-C bps require protonation of cytosine-N3 (Fig. 1a).

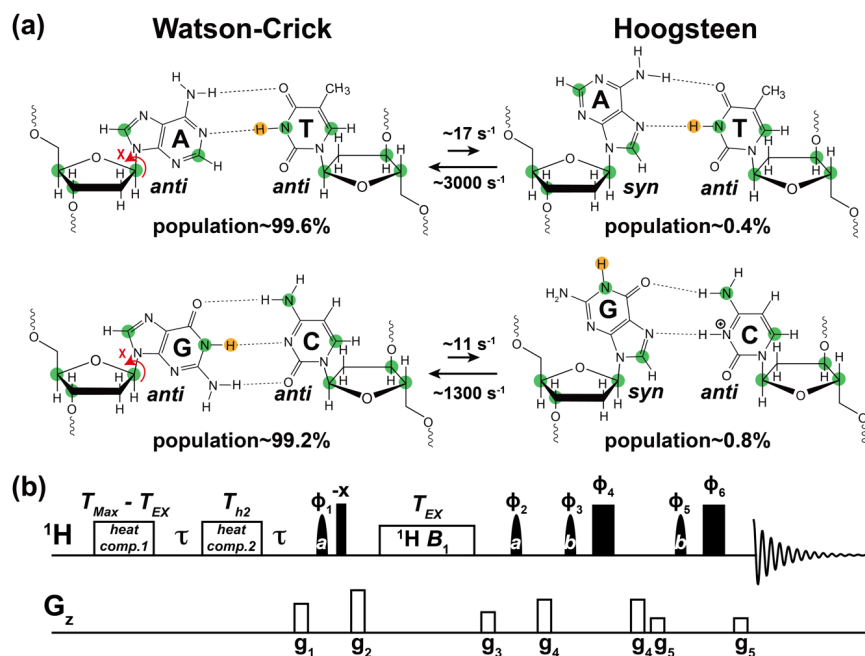


Figure 1. Using ^1H CEST to measure Watson-Crick to Hoogsteen exchange in unlabeled nucleic acid duplexes. (a) Watson-Crick G-C and A-T bps in B-DNA exist in dynamic equilibrium with G-C⁺ and A-T Hoogsteen bps, respectively. Filled green circles denote nuclei (^{13}C and ^{15}N) that have previously been used to probe the Watson-Crick to Hoogsteen exchange via RD measurements, while the yellow circle denotes the imino ^1H probes used in this study. Rate constants and populations were obtained as described previously (Alvey et al., 2014). (b) The 1D SELOPE ^1H CEST pulse sequence for characterizing chemical exchange in unlabeled nucleic acids. Narrow and wide filled rectangles denote 90° and 180°

hard pulses. Semi-oval shapes denote selective pulses. Pulse **a** is a 90°
 Eburp2.1000 shape pulse (typically 3-4 ms) for selective excitation (excitation
 bandwidth ~2-3 ppm) of imino protons, while pulse **b** is a 180° Squa100.1000
 shape pulse with length 2 ms in an excitation sculpting scheme (Hwang and
 Shaka, 1995) for water suppression. Open rectangles denote the gradients and
 heat compensation elements. Delay $\tau = \frac{1}{2} d_1 = 0.7$ s. To ensure uniform heating
 for experiments with variable lengths of T_{EX} , the relaxation period during which a
 1H B_1 field is applied, two heat compensation modules were used according to a
 prior study (Schlagnitweit et al., 2018). The first heat compensation is applied far
 off-resonance with duration = $T_{Max} - T_{EX} = 2$ ms, where T_{Max} is the maximum
 relaxation delay time. The second heat compensation (1 kHz) applied far off-
 resonance has a duration $T_{h2} = 150$ ms. The phase cycles used are $\phi_1 = \{8x, 8(-x)\}$,
 $\phi_2 = \{4x, 4(-x)\}$, $\phi_3 = \{x, y\}$, $\phi_4 = \{-x, -y\}$, $\phi_5 = \{2x, 2y\}$, and $\phi_6 = \{2(-x), 2(-y)\}$.
 Gradients (g1 - g5) with SMSQ10.100 profiles are applied for 1 ms with the
 following amplitudes (G cm⁻¹): 14.445, 26.215, 14.445, 16.585, 5.885. The 1H
 carrier is placed far offset (100,000 Hz) during the two heat compensation periods,
 then moved to the center of the imino resonances prior to the first pulse **a**. Next,
 the carrier is placed to a specified offset prior to the relaxation delay (T_{EX}), then
 placed back to the center of the imino resonances following T_{EX} . Finally, it is placed
 on-resonance with water for water suppression prior to pulse **b**. Briefly, imino 1H

magnetization is selectively excited, aligned longitudinally and then relaxes under a ^1H B_1 field during T_{EX} . ^1H transverse magnetization is then created and directly detected following water suppression. This pulse sequence is adapted from Schlagnitweit *et al* (Schlagnitweit et al., 2018).

Following their discovery, Hoogsteen bps were observed in crystal structures of duplex DNA in complex with proteins (Kitayner et al., 2010; Aishima et al., 2002) and drugs (Wang et al., 1984; Ughetto et al., 1985) and shown to play roles in DNA recognition (Golovenko et al., 2018), damage induction (Xu et al., 2020), and repair (Lu et al., 2010), and in damage bypass during replication (Nair et al., 2006; Ling et al., 2003). NMR relaxation dispersion (RD) studies employing off-resonance ^{13}C and ^{15}N spin relaxation in the rotating frame ($R_{1\rho}$) later showed that the G-C and A-T Watson-Crick bps exist in a dynamic equilibrium with their Hoogsteen counterparts (Nikolova et al., 2011). The Hoogsteen bps were shown to be lowly populated (population < 1 %) and short-lived (lifetime ~ 1 ms) forming robustly as an excited conformational state (ES) in duplex DNA across a variety of sequence contexts (Alvey et al., 2014) (Fig. 1a).

There is growing interest in mapping the Watson-Crick to Hoogsteen exchange landscape cross different DNA contexts, including for bps in different sequence

101 motifs (Alvey et al., 2014), near sites of damage and mismatches (Shi et al., 2021;
102 Singh et al., 1993), and when DNA is bound to proteins (Nikolova et al., 2013b;
103 Zhou et al., 2019) and drugs (Xu et al., 2018; Wang et al., 1984). Studies suggest
104 an increased propensity to form Hoogsteen bps in such environments (Shi et al.,
105 2021) and this may in turn play roles in DNA recognition and damage repair (Afek
106 et al., 2020). Furthermore, there is interest in understanding how the Hoogsteen
107 exchange varies with temperature (Nikolova et al., 2011), pH (Nikolova et al.,
108 2013a), salt concentration and buffer composition (Rangadurai et al., 2020b;
109 Tateishi-Karimata et al., 2014), as well as in the presence of epigenetic
110 modifications (Wang et al., 2017; Rangadurai et al., 2019a), all of which could
111 shape these dynamics and consequently DNA biochemical transactions.

112

113 There are hundreds and thousands of motifs and conditions for which
114 characterization of Hoogsteen dynamics is of biological interest. However, current
115 approaches for measuring Hoogsteen dynamics are ill-suited for dynamics
116 measurements at such a scale. The Watson-Crick to Hoogsteen chemical
117 exchange process has been characterized with the use of ^{13}C (Nikolova et al.,
118 2011; Shi et al., 2018; Ben Imeddourene et al., 2020; Alvey et al., 2014) and ^{15}N
119 (Nikolova et al., 2012a; Rangadurai et al., 2019a; Alvey et al., 2014) off-resonance
120 $R_{1\rho}$, and more recently chemical exchange saturation transfer (CEST) experiments

121 (Rangadurai et al., 2020b; Rangadurai et al., 2020a). However, these approaches
122 require isotopically enriched DNA samples, making broad explorations of
123 Hoogsteen exchange across even tens of motifs impractical. Furthermore, many
124 motifs of interest involve damaged or modified nucleotides, which are difficult to
125 isotopically enrich with ^{13}C and ^{15}N nuclei. It is therefore desirable to have more
126 facile means to initially assess Watson-Crick to Hoogsteen exchange, and to follow
127 up with in-depth characterization for those motifs exhibiting interesting and unusual
128 behavior. For such an initial screening application, we turned our attention to the
129 imino ^1H as a probe of the Watson-Crick to Hoogsteen exchange in unlabeled DNA
130 samples.

Deleted: It is for this reason that

131
132 The utility of protons as probes in CEST (Chen et al., 2016; Dubini et al., 2020;
133 Wang et al., 2021; Liu et al., 2020), Carr-Purcell-Meiboom-Gill (CPMG) (Juen et
134 al., 2016; Leblanc et al., 2018), and off-resonance $R_{1\rho}$ experiments (Wang and
135 Ikuta, 1989; Lane et al., 1993; Steiner et al., 2016; Schlagnitweit et al., 2018;
136 Baronti et al., 2020; Furukawa et al., 2021) to study conformational exchange in
137 nucleic acids is now well-established. Many of these ^1H based approaches use
138 experiments originally developed to study conformational exchange in proteins
139 (Ishima et al., 1998; Eichmuller and Skrynnikov, 2005; Lundstrom and Akke, 2005;
140 Lundstrom et al., 2009; Otten et al., 2010; Bouvignies and Kay, 2012; Hansen et

142 al., 2012; Weininger et al., 2012; Weininger et al., 2013; Smith et al., 2015; Sekhar
143 et al., 2016; Yuwen et al., 2017a; Yuwen et al., 2017b). The ^1H experiments permit
144 the use of higher effective fields allowing characterization of conformational
145 exchange faster than is possible using ^{13}C or ^{15}N experiments (Steiner et al., 2016;
146 Palmer, 2014). Furthermore, the relationship between ^1H chemical shifts and
147 structure is reasonably well understood and has been exploited in the
148 conformational characterization of nucleic acids (Sripakdeevong et al., 2014;
149 Frank et al., 2013; Wang et al., 2021; Swails et al., 2015; Czernek et al., 2000;
150 Lam and Chi, 2010).

151

152 Recently, ^1H $R_{1\rho}$ and CEST SElective Optimized Proton Experiments (SELOPE)
153 were developed and applied to characterize conformational exchange in unlabeled
154 RNA (Schlaginitweit et al., 2018). The SELOPE experiment has already found
155 several applications in studies of unlabeled nucleic acids, including in the
156 characterization of fast ($k_{\text{ex}} = k_1 + k_{-1} > 1,000 \text{ s}^{-1}$) RNA secondary structural
157 rearrangements (Baronti et al., 2020) and DNA base opening (Furukawa et al.,
158 2021), as well as slower ($k_{\text{ex}} < 100 \text{ s}^{-1}$) DNA hybridization kinetics (Dubini et al.,
159 2020). Many ^1H relaxation dispersion (RD) studies have targeted exchangeable
160 imino protons (Baronti et al., 2020; Furukawa et al., 2021), taking advantage of the

161 well-known dependence of the imino ^1H chemical shifts on secondary structure
162 (Wang et al., 2021; Lam and Chi, 2010).

163

164 Although ^1H RD experiments can obviate the need for isotopic labeling and offer
165 other advantages such as high sensitivity, they have not been as widely used
166 compared to $^{13}\text{C}/^{15}\text{N}$ RD experiments. One reason for this has to do with potential
167 artifacts arising due to from ^1H - ^1H cross relaxation (Ishima et al., 1998; Eichmuller
168 and Skrynnikov, 2005; Lundstrom and Akke, 2005; Bouvignies and Kay, 2012).
169 Interestingly, in nucleic acids, such NOE effects appear to be effectively
170 suppressed in the ^1H SELOPE experiment through selective excitation of spins
171 (Schlagnitweit et al., 2018). The exchange parameters obtained using ^1H SELOPE
172 experiments were shown to be in very good agreement with counterparts obtained
173 using ^{13}C and ^{15}N off-resonance $R_{1\rho}$ (Baronti et al., 2020). In addition, similar
174 exchange parameters were obtained when using variable tilt angles in $R_{1\rho}$
175 experiments, including tilt angle of 35.3° in which ROE and NOE cross-relaxation
176 terms cancel (Eichmuller and Skrynnikov, 2005; Weininger et al., 2013; Steiner et
177 al., 2016). No NOE dips or artifacts were observed in the majority of the ^1H CEST
178 or off-resonance $R_{1\rho}$ profiles (Steiner et al., 2016; Dubini et al., 2020; Furukawa et
179 al., 2021). These results are consistent with a prior off-resonance ^1H $R_{1\rho}$ studies
180 showing that even without deuteration, it is feasible to effectively suppress cross-

181 relaxation between amide and aliphatic protons through selective inversion of
182 amide protons and use of short spin lock relaxation delays (Lundstrom and Akke,
183 2005; Schlagnitweit et al., 2018). Nevertheless, NOE effects have been reported
184 for select sites in ^1H SELOPE studies of nucleic acids (Schlagnitweit et al., 2018),
185 and in ^1H CEST studies of proteins (Bouvignies and Kay, 2012; Sekhar et al., 2016;
186 Yuwen et al., 2017a; Yuwen et al., 2017b). This underscores the need to carefully
187 analyze NOE effects, especially for unlabeled samples, in which spin-state-
188 selective magnetization transfer schemes (Yuwen et al., 2017a; Yuwen et al.,
189 2017b) employing heteronuclei to suppress NOE effects are not feasible.

190

191 There are certain conditions in which the Hoogsteen bp becomes the dominant
192 conformation in duplex DNA. These include chemically modified bases (Nikolova
193 et al., 2011), when DNA is in complex with binding partners (Xu et al., 2018), and
194 for specific sequence contexts under certain experimental conditions (Stelling et
195 al., 2017). Based on NMR studies of such duplexes containing Hoogsteen bps,
196 there should be a sizeable difference ($\Delta\omega \sim 1 - 2$ ppm) between the imino proton
197 chemical shifts of guanine (G-H1) and thymine (T-H3) in the Hoogsteen versus
198 Watson-Crick conformation. These differences should render G-H1 and T-H3
199 suitable probes of Hoogsteen exchange in unlabeled DNA duplexes provided that
200 NOE effects can be effectively suppressed. Imino protons are also attractive

201 probes given that they are often well-resolved even in 1D ^1H spectra of large RNAs.

202 Since no other ESs have been detected to date in several NMR studies of
203 unmodified canonical DNA duplexes (Nikolova et al., 2011; Alvey et al., 2014; Shi
204 et al., 2018; Ben Imeddourene et al., 2020), a single imino ^1H probe could be
205 sufficient to reliably map and characterize the Watson-Crick to Hoogsteen
206 exchange.

207

208 Here, we show that high power ^1H CEST SELOPE experiments targeting the imino
209 protons G-H1 and T-H3 provide facile means for initially assessing Watson-Crick

Deleted: measuring

210 to Hoogsteen exchange of G-C and A-T bps in DNA without the need for isotopic
211 enrichment. NOE effects are shown to have a negligible contribution as short
212 (≤ 100 ms) relaxation delays can be used to characterize the relatively fast ($k_{\text{ex}} \sim$
213 500 to $8,000$ s^{-1}) Watson-Crick to Hoogsteen exchange process (Alvey et al., 2014).

214 The approach also takes advantage of high-power radio-frequency (RF) fields
215 recently shown (Rangadurai et al., 2020a) to extend the timescale sensitivity of
216 CEST to include faster exchange processes that traditionally are more effectively
217 characterized with the use of $R_{1\rho}$. The high-power ^1H CEST experiment also
218 enabled measurement of fast Hoogsteen exchange kinetics ($k_{\text{ex}} > 20,000$ s^{-1})
219 inaccessible to conventional ^{13}C or ^{15}N off-resonance $R_{1\rho}$ RD. The ^1H CEST
220 experiment opens the door to more comprehensively and systematically exploring

222 how the Watson-Crick to Hoogsteen exchange process varies with sequence and
223 structural contexts, and physiological conditions of interest.
224

2 Results

2.1 Assessment of NOE effects

We used the SELOPE (Schlaginitweit et al., 2018) experiment (Fig. 1b) to measure ^1H CEST profiles for G-H1 and T-H3 in unlabeled DNA duplexes (Fig. 2) at 25 °C-26 °C. We used ^1H CEST rather than $R_{1\rho}$ given the greater ease of collecting profiles for many spins simultaneously, and given that with the use of high-power RF fields, CEST can effectively characterize exchange processes over a wide range of timescales (Rangadurai et al., 2020a). Use of high power RF fields was recently shown to be important to effectively characterize the comparatively fast ($k_{\text{ex}} \sim 3,000 \text{ s}^{-1}$) Watson-Crick to Hoogsteen exchange process using ^{13}C and ^{15}N CEST experiments (Rangadurai et al., 2020a). Here, we also employed high power RF fields ($> 250 \text{ Hz}$) to optimally characterize Watson-Crick to Hoogsteen exchange using ^1H CEST.

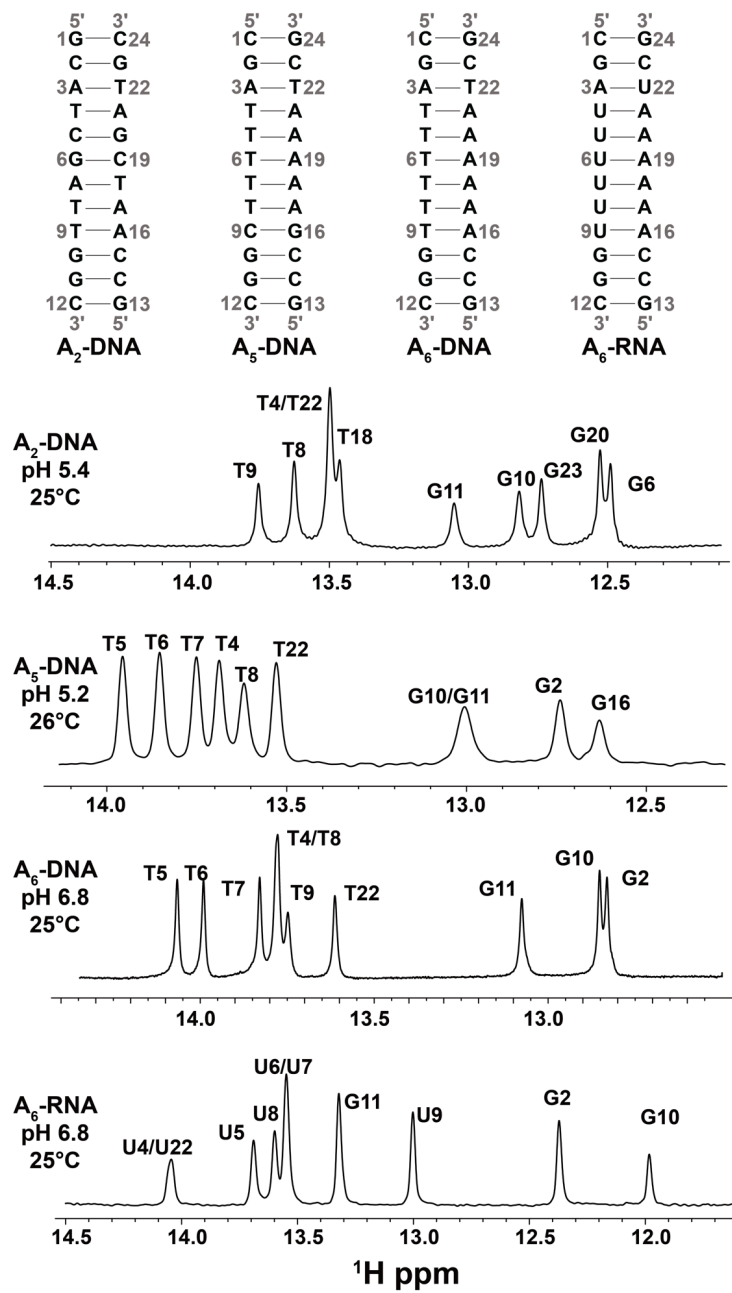


Figure 2. DNA and RNA duplexes used in this study. Also shown are 1D ^1H spectra of the imino region. The buffer conditions were 25 mM sodium chloride, 15 mM sodium phosphate, 0.1 mM EDTA and 10 % D_2O . The pH and temperature are indicated on each spectrum.

An important consideration when performing ^1H CEST experiments are contributions due to ^1H - ^1H cross-relaxation, which may give rise to extraneous NOE dips in the ^1H CEST profiles (Ishima et al., 1998; Lundstrom and Akke, 2005; Eichmuller and Skrynnikov, 2005; Bouvignies and Kay, 2012; Sekhar et al., 2016; Yuwen et al., 2017a; Yuwen et al., 2017b). These contributions have been suppressed in proteins through deuteration (Eichmuller and Skrynnikov, 2005; Lundstrom and Akke, 2005; Lundstrom et al., 2009; Otten et al., 2010; Hansen et al., 2012; Weininger et al., 2012), and in ^{15}N isotopically labelled proteins (Yuwen et al., 2017a; Yuwen et al., 2017b) and nucleic acids (Wang et al., 2021; Liu et al., 2020) using spin-state-selective magnetization transfer schemes, and through selective inversion of protons combined with use of short relaxation times (Lundstrom and Akke, 2005; Schlagnitweit et al., 2018).

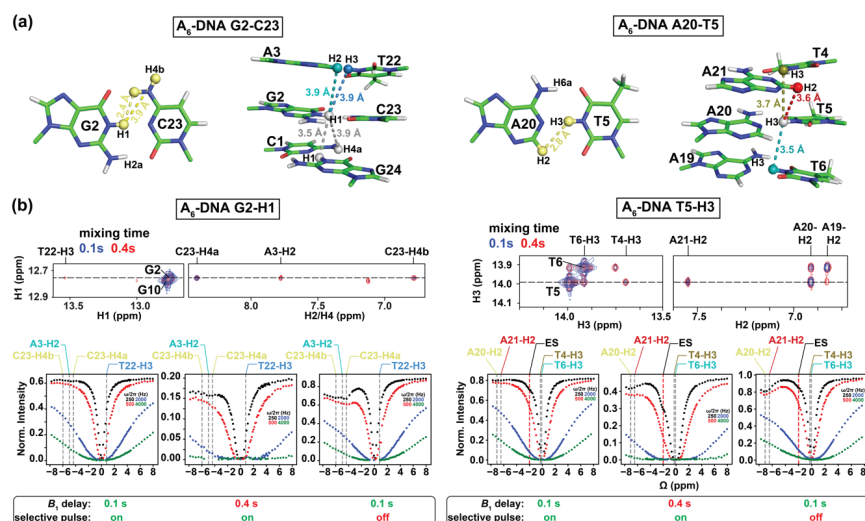
259 In the SELOPE experiment, imino protons are selectively excited and the
260 magnetization belonging to non-imino protons is dephased prior to application of
261 the B_1 field. This helps to suppress cross-relaxation (Yamazaki et al., 1994)
262 between the imino and non-imino protons (*vide infra*). In addition, because the
263 Watson-Crick to Hoogsteen exchange is relatively fast with $k_{ex} = \sim 500 - 8000 \text{ s}^{-1}$
264 at 25 °C (Alvey et al., 2014), we could afford to use a relatively short relaxation
265 delay of 100 ms which also helped minimize NOE effects (*vide infra*) (Lundstrom
266 and Akke, 2005; Schlagnitweit et al., 2018).

267

268 We initially performed experiments to evaluate contributions from ^1H - ^1H cross-
269 relaxation to the imino ^1H CEST profiles. In canonical B-form DNA and A-form
270 RNA duplexes (Fig. 2), G-H1 is in closest proximity to the partner base C-H4a
271 ($\sim 2.4 \text{ \AA}$, Fig. 3a), while T/U-H3 is in closest proximity to the partner A-H2 ($\sim 2.8 \text{ \AA}$,
272 Fig. 3a). Additional proximal protons include imino and H2 protons of neighboring
273 residues (~ 3.5 - 3.6 \AA , Fig. 3a). These short internuclear distances are reflected in
274 the intensity of cross peaks in 2D [^1H , ^1H] NOESY spectra of nucleic acid duplexes
275 (Fig. 3b and Fig. S1). Note that although the amino proton of G-H2a is in proximity
276 (2.2 \AA) to G-H1, while the amino proton of A-H6a is in proximity (2.4 \AA) to the
277 partner T-H3 (Fig. 3a), these amino protons are typically not observable in 1D ^1H

278 or 2D [$^1\text{H},^1\text{H}$] NOESY spectra caused by intermediate exchange due to the
 279 restricted rotation around the C-NH₂ bond (Schnieders et al., 2019).

280



281

282 **Figure 3. Analyzing NOE effects in ^1H CEST profiles.** (a) Distances between
 283 the imino protons of G2-H1 and T5-H3 and nearby protons in the A₆-DNA duplex
 284 (PDBID: 5UZF). Note that although the amino proton of G-H2a is in proximity (2.2
 285 Å) to G-H1, while the amino proton of A-H6a is in proximity (2.4 Å) to the partner
 286 T-H3, these amino protons are not observable in 1D ^1H or 2D [$^1\text{H},^1\text{H}$] NOESY
 287 spectra caused by intermediate exchange due to the restricted rotation around the
 288 C-NH₂ bond (Schnieders et al., 2019). (b) NOE dips in ^1H CEST profiles for G2-
 289 H1 and T5-H3 in A₆-DNA. The NOE diagonal and cross peaks for G2-H and T5-

290 H3 in the 2D [^1H , ^1H] NOESY spectra with mixing time 100 ms (blue) and 400 ms
291 (red) are shown on the top. The ^1H CEST profiles for G2-H1 and T5-H3 with
292 combinations of short (100 ms) and long (400 ms) relaxation delays, with and
293 without selective excitation (Methods) are shown at the bottom. The ES frequency
294 (black) obtained from fitting ^1H CEST profiles with selective excitation and short
295 relaxation delay (100 ms) as well as frequency positions corresponding to the NOE
296 cross peaks in the 2D [^1H , ^1H] NOESY spectra (top) are highlighted according to
297 the color scheme in (a) (bottom). Error bars for CEST profiles in (b), which are
298 smaller than the data points, were obtained using triplicate experiments, as
299 described in Methods. RF powers for CEST profiles are color-coded.

300

301 ^1H CEST profiles (Fig. 3b and Fig. S2) for well-resolved imino resonances of A₆-
302 DNA (Fig. 2) were acquired simultaneously in a 1D manner using ~3 hours of
303 acquisition time on a spectrometer operating at 600 MHz ^1H frequency equipped
304 with a cryogenic probe, and using ~1.0 mM unlabeled DNA (Methods). Data were
305 initially collected at pH = 6.8. Under these near neutral pH conditions, it is
306 generally not feasible to detect the Watson-Crick to Hoogsteen exchange process
307 for G-C bps due to the low population of the protonated G-C⁺ Hoogsteen bp
308 (Nikolova et al., 2013a). The lack of expected dips for the ES G-C⁺ Hoogsteen bp
309 under these conditions provides an opportunity to better assess any extraneous

310 ¹H CEST dips arising due to NOE effects. Unlike for G-C bps, the Hoogsteen
311 exchange should still be detectable for A-T bps under these pH conditions.

312

313 Shown in Fig. 3b is a representative imino ¹H CEST profile measured for G2-H1 in
314 the well-characterized A₆-DNA duplex (Nikolova et al., 2011). Besides the major
315 dip, no additional dips were visible in the ¹H CEST profile. The major dip was also
316 symmetric (Rangadurai et al., 2020a), indicating little to no contribution from
317 Hoogsteen exchange or NOE effects, as expected for G-C bps under these pH
318 conditions (Nikolova et al., 2013a). On the other hand, a minor shoulder was
319 observed in the ¹H CEST profile of T5-H3 (Fig. 3b, the $\Delta\omega$ is highlighted by a
320 dashed red line and labeled "ES"). The shoulder occurs at an offset frequency that
321 does not correspond with any other observable proton frequency in the A₆-DNA
322 duplex and is therefore unlikely to be the result of NOE effects (Fig. 3a). Rather,
323 as will be described below, the shoulder corresponds to the ES Hoogsteen bp
324 which is to be expected for the A-T bp at pH = 6.8.

325

326 To further verify that the dips observed in the ¹H CEST profile of T5-H3 and other
327 thymine residues in A₆-DNA (see Fig. 4 and S2) do not represent an NOE effect,
328 but rather reflect the ES Hoogsteen bp, we performed ¹H CEST experiments on a
329 corresponding A₆-RNA duplex (Fig. 2). Unlike in B-form DNA duplexes, G-C⁺ and

330 A-U Hoogsteen bps are both undetectable in A-form RNA duplexes by off-
331 resonance ^{13}C and ^{15}N $R_{1\rho}$ RD, most likely due their much lower population ($p_{\text{ES}} <$
332 0.04 %) (Zhou et al., 2016; Rangadurai et al., 2018). If the shoulder observed in
333 the ^1H CEST profile of T5-H3 in A₆-DNA is due to a Hoogsteen ES, and not NOE
334 dips, we would expect to observe a symmetric profile without ES dips for U5-H3 in
335 A₆-RNA. Indeed, the corresponding ^1H CEST profiles for U5-H3 (Fig. 4) and all
336 other uridine and guanine (Fig. S3) imino protons in A₆-RNA were symmetric, with
337 no evidence for any asymmetry or shoulder, indicating the absence of exchange
338 and NOE effects.

339

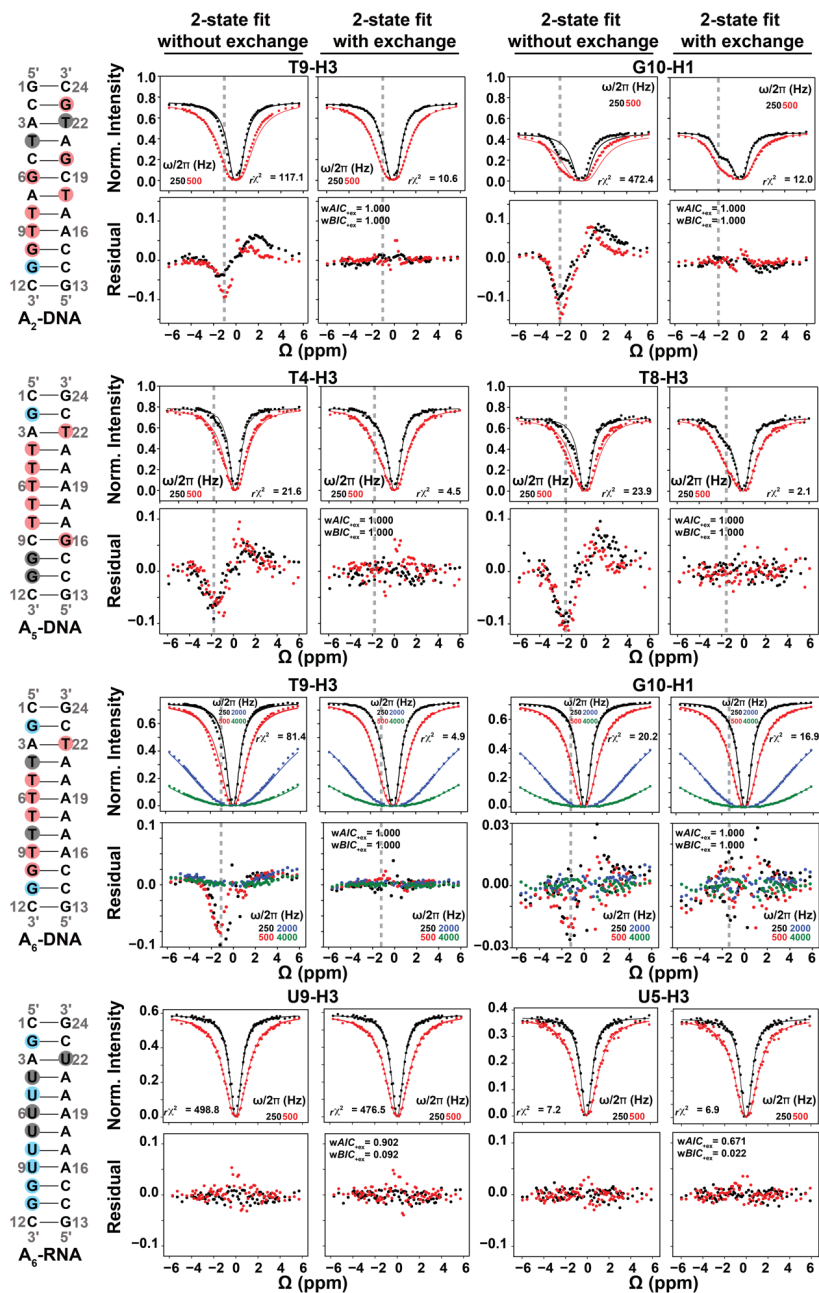


Figure 4. Representative ^1H CEST profiles measured for A₂-DNA (pH 5.4) at 25 °C, A₅-DNA (pH 5.2) at 26 °C, A₆-DNA (pH 6.8) at 25 °C and A₆-RNA (pH 6.8) at 25 °C. Residues with detectable RD, undetectable RD, and overlapped 1D ^1H resonances (see Fig. 2) are highlighted in red, blue, and gray circles respectively. Shown are the fits of the ^1H CEST data to a 2-state Bloch-McConnell equation with and without ($k_{\text{ex}} = \Delta\omega = p_{\text{ES}} = 0$) chemical exchange. Shown below the CEST profiles are residual (experimental normalized intensity - fitted normalized intensity) plots. Also shown in inset are the reduced chi-square ($r\chi^2$), and Akaike's (wAIC) and Bayesian information criterion (wBIC) weights for fits with exchange (Methods). The dashed gray lines indicate the Hoogsteen $\Delta\omega$ positions in both ^1H CEST profiles and in residual plots. Error bars for CEST profiles, which are smaller than the data points, were obtained using triplicate experiments, as described in Methods. RF powers for CEST profiles are color-coded.

Therefore, the shoulders in the ^1H CEST profiles (Fig. 3,4, Fig. S2,3) most likely rise due to chemical exchange with an ES. This was further confirmed by evaluating whether fits to the ^1H CEST profiles show any statistically significant improvement with the inclusion of exchange, as described below. Based on a similar analysis, no NOE dips were observable in the ^1H CEST profiles (Fig. 4, S2,3) for all other residues in A₆-DNA, A₆-RNA, and in two other DNA duplexes

across a range of pH and temperature conditions when using selective excitation and relaxation delay of 100 ms (Fig. 2, Fig. 4, and S2,3). These results indicate that any NOE effects between imino and non-imino protons are small under these experimental conditions.

Upon increasing the relaxation delay to 400 ms or using a non-selective ^1H excitation pulse (pulse **a** in Fig. 1b) with a delay of 100 ms, NOE dips became visible in the ^1H CEST profiles as shown for G2-H1 and T5-H3 (Fig. 3b) in A_6 -DNA. The dips occurred at the ^1H resonance frequency of nearby protons, and as expected, were particularly pronounced for the partner C-H4a in the case of G2-H1 and the partner A-H2 in the case of T5-H3 (Fig. 3b). Nevertheless, even the ^1H CEST profiles acquired with 400 ms delay could be fit when restricting the offset to the imino proton region (-3 - 3 ppm), and the fitted exchange parameters were similar to those obtained from fitting profiles with 100 ms relaxation delay in which no NOE dips were visible (Fig. S4, Table S1). In contrast, the ^1H CEST profiles measured using non-selective excitation, which had larger NOE dips relative to using a selective excitation pulse, could not be satisfactorily fit (Fig. S4).

No NOE dips were observed at the chemical shift of imino protons belonging to neighboring residues in ^1H CEST profiles measured in DNA and RNA duplexes,

Deleted:

NOE dips arising from cross-relaxation to neighboring imino protons (Fig. 3a) are more difficult to assess, as they would be buried within the major dip (Fig. 3b). However, since no NOE dips were observable for non-imino protons within 2.8 Å (Fig. 3a), a sizeable cross-relaxation contribution from neighboring imino protons is unlikely considering they are separated by a longer internuclear distance of ~3.7-3.9 Å (Fig. 3a), and correspondingly, have weaker intensities in 2D NOESY spectra (Fig. 3b). Nevertheless, whether or not these NOE effects are large enough to impact determination of the exchange parameters was examined (*vide infra*) through comparison of the exchange parameters derived from fitting the imino- ^1H CEST profiles with those measured independently using off-resonance- ^{13}C and ^{15}N $R_{1\rho}$ RD measurements.

and none of the ^1H CEST profiles collected in this study yielded an ES with $\Delta\omega$ compatible with the imino ^1H chemical shift of a neighboring residue. Nevertheless, these NOE effects could be more difficult to assess given that they would be buried within the major dip. While imino-imino ^1H NOEs are not suppressed by selective excitation, their contribution is expected to be smaller relative to other NOE dips observed when using non-selective excitation (distances $\sim 2.4 - 2.8 \text{ \AA}$ between guanosine/thymine imino and cytosine amino/adenine H2) due to the larger distance of separation between neighboring imino protons ($\sim 3.5 - 3.9 \text{ \AA}$) (Fig. 3a).

To further assess the impact of imino-imino ^1H NOEs on the ^1H CEST profiles, we examined whether selective excitation of imino protons (but not their immediate neighbors) results in different ^1H CEST profiles relative to an experiment in which all imino protons are excited. We performed an experiment selectively exciting G10-H1 and G2-H1 in A₆-DNA without exciting the imino resonances belonging to either of their two immediate neighbors. Selective excitation of individual imino protons resulted in ^1H CEST profiles (Fig. S2) and fitted parameters (Table S1) for G10-H1 and G2-H1 that are within error to those obtained when exciting all imino protons, again indicating that any imino-imino NOE contribution is negligible. Finally, the impact of imino-imino NOEs on the determination of the exchange

parameters was also assessed (*vide infra*) through comparison of the exchange parameters derived from fitting the imino ^1H CEST profiles with those measured independently using off-resonance ^{13}C and ^{15}N $R_{1\rho}$ RD measurements.

These results underscore the importance of critically evaluating the NOE contributions on a case-by-case basis (Schlagnitweit et al., 2018) and also suggest that NOE effects can be effectively suppressed for the canonical duplexes used in this study provided use of selective excitation and short relaxation delays.

It should be noted that to avoid any complexities due to NOE effects with water protons or hydrogen exchange, we restricted the offset to -6 ppm to 6 ppm when analyzing and fitting the ^1H CEST profiles. This is common practice as relatively narrow offsets (< 4 ppm) were used in prior ^1H CEST studies of both nucleic acids (Dubini et al., 2020; Wang et al., 2021; Liu et al., 2020) and proteins (Yuwen et al., 2017a; Yuwen et al., 2017b). While we did not observe a dip near the water chemical shift in the ^1H CEST profile for the internal residue T5-H3, a weak and broad dip near the water chemical shift was observed in the profile for the near terminal residue G2-H1 (Fig. S2). The latter dip could be due to NOEs between G2-H1 and water protons and/or due to fast hydrogen exchange kinetics.

2.2 Benchmarking the utility of ^1H CEST to probe Watson-Crick to Hoogsteen exchange in DNA duplexes

To examine the utility of the SELOPE ^1H CEST experiment to characterize Watson-Crick to Hoogsteen exchange, we benchmarked the experiment by measuring conformational exchange in three DNA duplexes ($\text{A}_6\text{-DNA}$, $\text{A}_2\text{-DNA}$ and $\text{A}_5\text{-DNA}$, Fig. 2) for which we have previously extensively characterized the Watson-Crick to Hoogsteen exchange using ^{13}C and ^{15}N off-resonance $R_{1\rho}$ (Nikolova et al., 2011; Alvey et al., 2014; Shi et al., 2018) and CEST (Rangadurai et al., 2020a; Rangadurai et al., 2020b) experiments. We compared the exchange parameters derived using ^1H CEST with counterparts derived using $^{13}\text{C}/^{15}\text{N}$ $R_{1\rho}$ or CEST for a variety of G-C and A-T bps across three different DNA duplexes and varying pH (5.2-6.8) conditions. All ^1H CEST experiments were performed using 100 ms relaxation delay and selective excitation.

As expected, for several thymine residues, the imino ^1H CEST profile was visibly asymmetric (Fig. 4 and Fig. S2,3), consistent with relatively fast ($k_{\text{ex}} > 1000 \text{ s}^{-1}$) Watson-Crick to Hoogsteen exchange. The asymmetry manifests as an upfield shifted shoulder (e.g. T8-H3 in $\text{A}_5\text{-DNA}$ in Fig. 4) as expected for T-H3 Hoogsteen chemical shift ($\Delta\omega \sim 2 \text{ ppm}$) (Nikolova et al., 2011; Xu et al., 2018). In other cases, such as T9-H3 in $\text{A}_6\text{-DNA}$, the asymmetry was less pronounced, and the exchange

458 contribution was only apparent following comparison of fits with and without
459 exchange (see Fig. 4).

460

461 As expected, at pH = 6.8, the imino ^1H CEST profiles were symmetric for most
462 guanine residues consistent with no observable exchange (Fig. 4 and S2,3).
463 However, the major dip became asymmetric for several guanine residues when
464 lowering the pH to 5.2 or 5.4, as expected for the Watson-Crick to Hoogsteen
465 exchange of G-C bps, which is favored at lower pH (Fig. 4 and S3). All minor dips
466 occurred at resonance frequencies that did not correspond with any other protons
467 in the molecule (Fig. 2 and S1,2). In all cases, the ^1H CEST profiles could be
468 satisfactorily fit to a 2-state model with or without exchange, suggesting that any
469 NOE contribution to the ^1H CEST profile is likely to be insignificant.

470

471 To identify which imino ^1H CEST profiles have significant chemical exchange
472 contributions, each profile was subjected to a fit with or without ($\Delta\omega = p_{\text{ES}} = k_{\text{ex}} =$
473 0) 2-state chemical exchange (Methods). Akaike information criterion (AIC) and
474 Bayesian information criterion (BIC) (Burnham and Anderson, 2004) weights were
475 then used to evaluate whether any improvement in the fit due to inclusion of
476 chemical exchange was statistically significant (Kimsey et al., 2018; Liu et al.,
477 2020). The improvement of fit was considered to be statistically significant when

478 both AIC and BIC weights > 0.995 and the reduced chi-square ($r\chi^2$) is reduced
479 with the inclusion of exchange. Residual plots were also used to visualize changes
480 in fit quality (Fig. 4).

481

482 Based on the AIC and BIC analysis, all thymine and guanine residues shown
483 previously to undergo Watson-Crick to Hoogsteen exchange using off-resonance
484 ^{13}C and/or ^{15}N $R_{1\rho}$ under these experimental conditions, also showed statistically
485 significant improvements when fitting the ^1H CEST profiles with the inclusion of
486 chemical exchange (Fig. 4 and S2,3). On the other hand, all guanine residues
487 including G2 and G11 in A_6 -DNA and G11 in A_2 -DNA, which did not show signs of
488 Hoogsteen exchange in off-resonance ^{13}C and/or ^{15}N $R_{1\rho}$ (Nikolova et al., 2011;
489 Shi et al., 2018) under these experimental conditions also did not show statistically
490 significant improvements when fitting their ^1H CEST profiles with the inclusion of
491 chemical exchange (Fig. 4 and S2,3).

492

493 Interestingly, a few residues including T5, T6, T7 and T22 in A_6 -DNA, T18, G6 and
494 G20 in A_2 -DNA (Fig. S2,3), showed exchange based on ^1H CEST but did not show
495 evidence for Hoogsteen exchange based on prior off-resonance ^{13}C and/or ^{15}N $R_{1\rho}$
496 experiments (Nikolova et al., 2011; Alvey et al., 2014; Shi et al., 2018). As will be
497 elaborated in the following section, these data provide new insights into the

498 Watson-Crick to Hoogsteen exchange process, and suggest that at least in some
499 cases, ^1H CEST can exceed the detection limits of $^{13}\text{C}/^{15}\text{N}$ based methods.

500

501 In addition, T18 and G20 in A_2 -DNA were difficult to probe using ^{13}C RD due to
502 spectra overlap (Nikolova et al., 2011) but could easily be measured using ^1H
503 CEST (Fig. 2, 4 and S3). In contrast, other residues such as T8 and T4 in A_6 -DNA,
504 T4 and T22 in A_2 -DNA, and G10 and G11 in A_5 -DNA could be targeted for ^{13}C or
505 ^{15}N RD measurements (Nikolova et al., 2011; Alvey et al., 2014) but could not be
506 measured by ^1H CEST due to overlap in the 1D ^1H imino spectra (Fig. 2). This
507 highlights the complementarity of ^1H and $^{13}\text{C}/^{15}\text{N}$ RD in characterizing Watson-
508 Crick to Hoogsteen exchange.

509

510 To assess how well the exchange parameters are determined by the ^1H CEST
511 data, we subjected the ^1H CEST profiles for residues T7 ($k_{\text{ex}}/\Delta\omega \sim 0.2$), T9 ($k_{\text{ex}}/\Delta\omega$
512 ~ 0.82) and T22 ($k_{\text{ex}}/\Delta\omega \sim 3.5$) which exhibit exchange on the slow, intermediate,
513 and fast timescale (Rangadurai et al., 2019b) respectively, to a degeneracy
514 analysis. We computed the reduced chi-square ($r\chi^2$) for a 2-state fit as a function
515 of varying k_{ex} , $\Delta\omega$ or p_{ES} . In all cases, the $r\chi^2$ values increased significantly (up
516 to 10-fold) when varying k_{ex} , $\Delta\omega$ or p_{ES} by 3-fold (Fig. S5), indicating that the
517 exchange parameters are well-defined by the ^1H CEST data.

To test the accuracy of the exchange parameters obtained using ^1H CEST, we compared the exchange parameters p_{ES} and k_{ex} , derived from a 2-state fit of the data to values determined previously using off-resonance ^{13}C and/or ^{15}N $R_{1\rho}$ (Nikolova et al., 2011; Shi et al., 2018; Alvey et al., 2014) for Hoogsteen dynamics (Fig. 5a and Table S1). In total, we were able to compare 13 data points from ^1H CEST and $^{13}\text{C}/^{15}\text{N}$ $R_{1\rho}$ for three different duplexes under different conditions of temperature and pH (Fig. 2,5a). This comparison also allowed us to further verify that the exchange process detected by ^1H CEST does indeed correspond Watson-Crick to Hoogsteen exchange, and to also further assess for potential contributions from NOE effects, which might cause deviations from agreement.

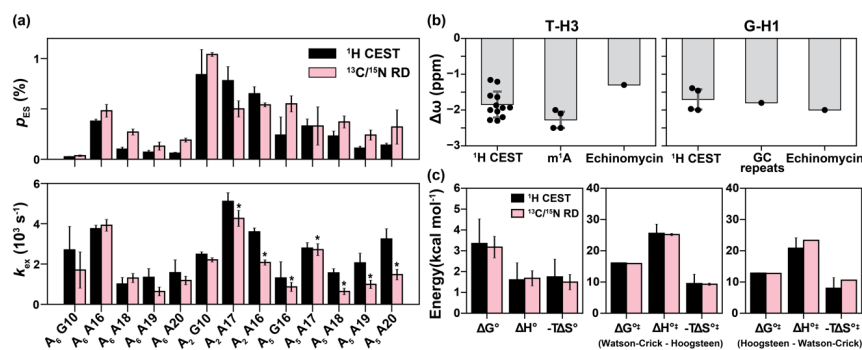


Figure 5. Comparison of exchange parameters for the Watson-Crick to Hoogsteen exchange obtained from ^1H CEST and $^{13}\text{C}/^{15}\text{N}$ $R_{1\rho}$. (a) Comparison of

533 exchange parameters (k_{ex} and p_{ES}) measured using ^1H CEST with counterparts
 534 previously reported using $^{13}\text{C}/^{15}\text{N}$ off-resonance $R_{1\rho}$ (Nikolova et al., 2011; Alvey
 535 et al., 2014; Shi et al., 2018). ^{13}C RD data for A18, A19 and A20 were measured
 536 using off-resonance $R_{1\rho}$ in this study (Fig. S7). Small systematic deviations in k_{ex}
 537 for the values indicated with asterisks could be due to small differences in
 538 temperature ($< 0.8^\circ\text{C}$) across different spectrometers. Bps are specified by the
 539 corresponding purine residue. (b) Comparison of the $\Delta\omega$ obtained from fitting ^1H
 540 CEST profiles for T-H3 and G-H1 (Table S1) with the values expected for a
 541 Watson-Crick to Hoogsteen transition based on duplexes in which A-T or G-C⁺
 542 Hoogsteen bps were rendered the dominant state, by using N^1 -methylated adenine
 543 ($m^1\text{A}$) (Nikolova et al., 2011; Sathyamoorthy et al., 2017; Rangadurai et al.,
 544 2020b), by binding of the drug (echinomycin) to a DNA duplex (Xu et al., 2018),
 545 or through use of GC repeat sequences (GC repeats) that predominantly form
 546 Hoogsteen bps at low pH (Stelling et al., 2017). (c) Comparison of free energy
 547 (ΔG°), enthalpy (ΔH°) and entropy ($-\Delta S^\circ$, $T = 25^\circ\text{C}$) of the Watson-Crick to
 548 Hoogsteen transition, and the activation free energy ($\Delta G^{\circ\dagger}$), enthalpy ($\Delta H^{\circ\dagger}$) and
 549 entropy ($-\Delta S^{\circ\dagger}$, $T = 25^\circ\text{C}$) for Watson-Crick to Hoogsteen (Watson-Crick -
 550 Hoogsteen) and Hoogsteen to Watson-Crick (Hoogsteen - Watson-Crick)
 551 transitions measured using ^1H CEST in this study and using ^{13}C $R_{1\rho}$ from Nikolova
 552 et al (Nikolova et al., 2011). The energetics in (c) were measured for the Watson-

553 Crick to Hoogsteen transition of A16-T9 in A₆-DNA at pH 6.8. Errors in (a) were
554 fitting errors of ¹H CEST, calculated as described in Methods or errors of ¹³C/¹⁵N
555 *R*_{1ρ} calculated using a Monte-Carlo scheme as described previously (Rangadurai
556 et al., 2019b). Errors in (b) are the standard deviations of data points (shown as
557 black dots) in each category. Error bars in (c) were propagated from the errors in
558 the exchange parameters obtained from ¹H CEST or ¹³C/¹⁵N *R*_{1ρ}.

559

560

561 Indeed, the *p*_{ES} and *k*_{ex} values derived using ¹H CEST were in very good
562 agreement with their off-resonance ¹³C and/or ¹⁵N *R*_{1ρ} counterparts (Fig. 5a). The
563 differences between *k*_{ex} and *p*_{ES} measured using the two methods was often within
564 error with the largest differences being <3-fold. A small and systematic difference
565 in *k*_{ex} was observed for a subset of the data (Fig. 5a), and this might be due to
566 small temperature differences (<0.8°C) between spectrometers. Importantly, the
567 ES imino ¹H chemical shifts deduced from a 2-state fit of the ¹H CEST profiles
568 ($\Delta\omega_{A-T} = \sim -1$ to -2 ppm and $\Delta\omega_{G-C} = \sim -1.5$ to -2.0 ppm) were also in good agreement
569 with the expected range of values ($\Delta\omega = -1$ to -2 ppm) for Hoogsteen bps (Fig. 5b)
570 based on studies of duplexes containing Hoogsteen bps as the dominant
571 conformation (Nikolova et al., 2011; Stelling et al., 2017; Xu et al., 2018;
572 Rangadurai et al., 2020b).

573

574 As an additional test, we also measured temperature-dependent (5 °C, 10 °C,
575 20 °C, 25 °C, 30 °C and 45 °C) ^1H CEST profiles for $\text{A}_6\text{-DNA}$ at pH 6.8 (Fig. S2),
576 and then used the temperature dependence of the fitted kinetic rate constants (k_1
577 and k_{-1}) to determine the standard and activation enthalpy and entropy changes
578 for the Watson-Crick to Hoogsteen transition (Fig. S6). These values were in
579 excellent agreement with those measured from off-resonance ^{13}C $R_{1\rho}$ (Nikolova et
580 al., 2011) (Fig. 5c), further supporting the robustness of the ^1H CEST methodology.

581

582 **2.3 New insights into Hoogsteen breathing**

583 ^1H CEST profiles for some residues show detectable exchange contributions when
584 corresponding $^{13}\text{C}/^{15}\text{N}$ RD measurements do not or show only weak exchange.
585 This suggests that ^1H CEST can provide additional insights into Watson-Crick to
586 Hoogsteen exchange and extend the detection limits of conventional $^{13}\text{C}/^{15}\text{N}$ RD
587 measurements.

588

589 For example, using ^1H CEST it was feasible to measure Watson-Crick to
590 Hoogsteen exchange for T5-H3, T6-H3, and T7-H3 (Fig. S2) within the middle of
591 the A-tract motif (defined as $\text{A}_n\text{-tract}$ with $n>3$) in $\text{A}_6\text{-DNA}$. These residues had

592 previously exhibited only weak on-resonance ^{13}C $R_{1\rho}$ RD, and as a result, no off-
593 resonance $R_{1\rho}$ data were ever recorded (Nikolova et al., 2011). Based on the ^1H
594 CEST measurements, residues within the A-tract motif have ten-fold lower
595 Hoogsteen population ($p_{\text{ES}} = 0.06 \pm 0.01 \%$ - $0.09 \pm 0.03 \%$) relative to other A-T bps
596 in A₆-DNA ($p_{\text{ES}} > \sim 0.10 \%$) (Table S1). These represent the lowest A-T Hoogsteen
597 populations ever recorded to date in duplex DNA (Table S1). The exchange
598 kinetics were also 2-fold slower ($k_{\text{ex}} \sim 1000 \text{ s}^{-1}$) for the A-tract residues relative to
599 other A-T bps ($k_{\text{ex}} > 2000 \text{ s}^{-1}$) in A₆-DNA (Table S1). Interestingly, the suppression
600 of Hoogsteen dynamics within the A-tract motif appears to be A-tract length
601 dependent, with both the Hoogsteen population and exchange kinetics increasing
602 slightly for similar bps in A₅-DNA (Table S1). The suppression of Hoogsteen
603 dynamics within A-tracts is consistent with prior studies showing them to be more
604 rigid and stiff motifs relative to scrambled DNA (Nikolova et al., 2012b). We
605 verified these ^1H CEST derived exchange parameters for A-tract residues in A₆-
606 DNA by performing off-resonance ^{13}C $R_{1\rho}$ measurements (Fig. S7) on uniformly
607 $^{13}\text{C}/^{15}\text{N}$ labeled A₆-DNA and did indeed observe the expected RD with p_{ES} and k_{ex}
608 values similar (difference <3-fold, Fig. 5a) to those measured using ^1H CEST.
609 These prospective tests of the ^1H CEST data using off-resonance $^{13}\text{C}/^{15}\text{N}$ $R_{1\rho}$ RD
610 data further support the methodology.

611

612 The ability to characterize fast exchange kinetics has long been a motivation for
613 using ^1H in RD experiments to characterize conformational exchange (Ishima et
614 al., 1998; Ishima and Torchia, 2003; Eichmuller and Skrynnikov, 2005; Lundstrom
615 and Akke, 2005; Otten et al., 2010; Hansen et al., 2012; Smith et al., 2015; Steiner
616 et al., 2016; Furukawa et al., 2021). Indeed, ^1H CEST made it possible to measure
617 fast Watson-Crick to Hoogsteen exchange kinetics which were undetectable by
618 off-resonance ^{13}C $R_{1\rho}$. In particular, it was possible to measure Watson-Crick to
619 Hoogsteen exchange for T22 in A₆-DNA with $k_{\text{ex}} > 20,000 \text{ s}^{-1}$ (Fig. S2 and Table
620 S1), which is the fastest ever recorded Hoogsteen exchange process at 25 °C
621 (Table S1). In contrast, the off-resonance ^{13}C $R_{1\rho}$ RD profiles reported for this
622 residue in prior studies were flat (Nikolova et al., 2011; Shi et al., 2018), and
623 simulations show that such an exchange process is too fast for reliable detection
624 using ^{13}C $R_{1\rho}$ (Fig. S8a). Similarly, it was feasible to measure Watson-Crick to
625 Hoogsteen exchange for G6 ($p_{\text{ES}} \sim 0.3 \%$, $k_{\text{ex}} \sim 3000 \text{ s}^{-1}$) in A₂-DNA using ^1H CEST
626 yet no off-resonance ^{13}C $R_{1\rho}$ RD on C1' was previously detected (Shi et al., 2018),
627 which based on simulations, was likely due to a combination of exchange kinetics
628 and small $\Delta\omega$ value (Fig. S8b).

629

630 One of the potential utilities of the ^1H CEST experiment is the measurement of very
631 fast exchange kinetics at high temperatures and in a manner insensitive to melting

632 of duplexes, shown previously to complicate analysis of Hoogsteen exchange
633 using ^{13}C and ^{15}N RD (Shi et al., 2019). Melting of duplexes should not yield any
634 exchange dips around the imino ^1H region given that the imino protons of single-
635 stranded species (ssDNA) exchange rapidly with solvent.

636

637 We therefore measured ^1H CEST profiles for A_6 -DNA at 45°C (Fig. S2), in which
638 the ssDNA population is $\sim 10\%$ (Shi et al., 2019). We did not observe any evidence
639 for the ssDNA species in the ^1H CEST profiles. Instead, we were able to observe
640 ultra-fast ($k_{\text{ex}} \sim 10,000\text{ s}^{-1}$, see Table S1) Hoogsteen exchange which could not
641 previously be detected by ^{13}C or ^{15}N RD experiments at the same temperature (Shi
642 et al., 2019).

643

644 Taken together, these results demonstrate that the ^1H CEST experiment broadens
645 the range of populations and exchange rates over which Hoogsteen breathing can
646 be effectively characterized.

647 **3 Discussion**

648 Building on prior studies showing the utility of the SELOPE ^1H RD experiment in
649 measuring conformational exchange in unlabeled RNA (Schlagnitweit et al., 2018)

650 and DNA (Furukawa et al., 2021; Dubini et al., 2020), our study establishes the
651 utility of high-power ^1H CEST SELOPE as a facile means for rapidly assessing the
652 Watson-Crick to Hoogsteen exchange process in nucleic acids without the need
653 for isotopic enrichment. The methodology is supported by the very good
654 agreement observed between the measured exchange parameters and values
655 measured independently using ^{13}C and/or ^{15}N $R_{1\rho}$ for a variety of bps in three
656 duplexes under different conditions of temperature and pH, as well as by the good
657 agreement seen between the imino ^1H chemical shifts and those expected based
658 on duplexes containing Hoogsteen bps as the dominant GS conformation. The
659 high throughput nature of the experiment and simple sample requirements enabled
660 us to measure Hoogsteen dynamics for 37 data points corresponding to 22 distinct
661 bps for three different pH conditions and seven different temperatures (Table S1),
662 the largest collection of Hoogsteen dynamics from a single study to date. We
663 envision using the ^1H CEST SELOPE experiments to pre-screen DNA duplexes
664 and to perform follow-up ^{13}C and ^{15}N RD experiments to confirm any interesting
665 outliers, particularly regions showing substantially elevated Hoogsteen dynamics.
666
667 An important consideration when applying ^1H CEST to the study of chemical
668 exchange are contributions due to ^1H - ^1H cross-relaxation originating from cross
669 relaxation, which may give rise to extraneous NOE dips that complicate data

Deleted: measuring

671 analysis (Yuwen et al., 2017a; Bouvignies and Kay, 2012; Eichmuller and
672 Skrynnikov, 2005). These contributions have been shown to be significant in
673 proteins particularly when characterizing slow exchange ($k_{ex} < 200 \text{ s}^{-1}$)
674 necessitating use of relatively long relaxation delays (Bouvignies and Kay, 2012).
675 Consistent with prior studies of nucleic acids (Schlaginitweit et al., 2018; Steiner et
676 al., 2016; Baronti et al., 2020) and proteins (Lundstrom and Akke, 2005). Our
677 results indicate that NOE effects from cross-relaxation between imino and non-
678 imino protons can be effectively suppressed for DNA and RNA duplexes in the ^1H
679 CEST experiments through selective excitation provided that the relaxation delays
680 are short on the order of 100 ms (Fig. 3b). However, care should be exercised to
681 assess imino-imino NOE effects (Fig. 3b), which may also be more substantial for
682 certain non-canonical motifs. Data should be discarded if the ES chemical shifts
683 match those of nearby imino protons identified using 2D [^1H , ^1H] NOESY
684 experiments or if the magnitude of the dip of interest varies substantially with or
685 without selective excitation, as this could be an indication of NOE effect. Finally,
686 we recommend independent verification of the exchange parameters with the use
687 of other methods such as ^{13}C and ^{15}N experiments for motifs exhibiting highly
688 unusual exchange parameters or ES ^1H chemical shifts, and this can also help to
689 confirm Hoogsteen bps as the ES.

Deleted: ,

692 Prior studies showed that Watson-Crick to Hoogsteen bp transitions exhibit large
693 variations in the forward rate constants (k_1) while the backward rate constants (k_{-1})
694 is relatively constant across different sequence contexts, consistent with a late
695 transitional state (Alvey et al., 2014). We observe a similar trend in which k_{-1} varied
696 <5-fold while k_1 varied by ~50-fold (Fig. S9). The ^1H CEST data also revealed
697 significantly lower Hoogsteen abundance ($p_{\text{ES}} < 0.1\%$) in addition to slower
698 exchange kinetics ($k_{\text{ex}} \sim 1,000\text{ s}^{-1}$) within A-tract motifs (Nikolova et al., 2011; Alvey
699 et al., 2014), while also reinforcing prior data (Xu et al., 2018) suggesting increased
700 exchange kinetics near terminal ends. Collectively, these data show that the
701 Hoogsteen population can vary by as much as ~14-fold while k_{ex} can vary by ~20-
702 fold only due to changes in sequence and positional context (Table S1). These
703 strong sequence and position dependencies could play important roles in
704 biochemical processes acting on DNA.

705

706 A recent study (Furukawa et al., 2021) reported on-resonance imino ^1H $R_{1\rho}$ RD for
707 a guanine residue in a DNA duplex at pH = 7.5, T= 30 °C, and in 150 mM NaCl.
708 Because off-resonance measurements were not performed, only $k_{\text{ex}} \sim 10,000\text{ s}^{-1}$
709 could be determined while the values of $\Delta\omega$ and p_{ES} were not determined. The
710 study noted that a Hoogsteen bp as the ES was unlikely given that G-C⁺ Hoogsteen
711 bps are disfavored at pH= 7.5 and because the observed rate of exchange ($k_{\text{ex}} \sim$

712 10,000 s⁻¹) was much faster than is typically observed for Watson-Crick to
 713 Hoogsteen exchange. Instead, the data were interpreted as evidence for a base
 714 opened state. However, the observed rate of exchange $k_{\text{ex}} \sim 10,000 \text{ s}^{-1}$ falls
 715 comfortably within the range of values measured here for Watson-Crick to
 716 Hoogsteen exchange using ¹H CEST at similar pH conditions. For example, for
 717 the G10-C15 bp in A₆-DNA at the same temperature and pH = 6.8, k_{ex} for Watson-
 718 Crick to Hoogsteen exchange was $\sim 6,000 \text{ s}^{-1}$ (Fig. 4 and Table S1). Similar
 719 Watson-Crick to Hoogsteen exchange parameters ($p_{\text{ES}} \sim 0.05 \%$ and $k_{\text{ex}} \sim 2000 \text{ s}^{-1}$)
 720 were recently reported for this bp at 25 °C and pH 6.8 using cytosine amino ¹⁵N
 721 RD (Rangadurai et al., 2019a) and the ES $\Delta\omega_{\text{C-N4}} = -9 \text{ ppm}$ was shown to be in
 722 excellent agreement with values expected for a G-C⁺ Hoogsteen bp. In addition,
 723 based on hydrogen exchange measurements, $p_{\text{ES}} \sim 0.00001 \%$ to 0.01% and k_{ex}
 724 ($k_{\text{cl}} + k_{\text{op}}$, k_{cl} and k_{op} are the base closing and opening rate constant, respectively)
 725 $\sim 10^5$ to 10^7 s^{-1} for the base-opened ES, and this process should fall outside RD
 726 detection (Gueron and Leroy, 1995; Gueron et al., 1987; Leroy et al., 1988; Leijon
 727 and Graslund, 1992; Snoussi and Leroy, 2001). Therefore, the ES detected by
 728 Furukawa *et al* (Furukawa et al., 2021) is more likely a Hoogsteen bp.

729

730 In conclusion, by obviating the need for isotopic enrichment, the ¹H CEST
 731 experiment expands the scope of characterizing Watson-Crick to Hoogsteen

732 exchange in nucleic acids by NMR. We are presently applying the experiment to
733 map the sequence dependence of Hoogsteen breathing dynamics and
734 systematically, how it varies with pH, salt, and crowding, and following the
735 introduction of lesions, mismatches, and molecules that bind to the DNA.

4 Methods

4.1 Sample preparation

Unlabeled DNA and RNA oligonucleotides: Unmodified DNA oligonucleotides were purchased from Integrated DNA Technologies with standard desalting purification. RNA oligonucleotides were synthesized using a MerMade 6 Oligo Synthesizer employing 2'-tBDSilyl protected phosphoramidites (n-acetyl protected rC, rA and rG, and rU phosphoramidites were purchased from Chemgenes) and 1 μ mol standard synthesis columns (1000 Å) (BioAutomation). RNA oligonucleotides were synthesized with the final 5'-protecting group, 4,4'-dimethoxytrityl (DMT) retained. RNA oligonucleotides were cleaved from columns using 1 ml AMA (1:1 ratio of 30 % ammonium hydroxide and 30 % methylamine) and incubated at room temperature for 2 hours. The sample was then air-dried and dissolved in 115 μ L DMSO, 60 μ L TEA, and 75 μ L TEA.3HF, and then incubated at T = 65 °C for 2.5 hours to remove 2'-O protecting groups. The Glen-Pak RNA cartridges (Glen Research Corporation) were then used to purify the samples followed by ethanol precipitation.

Labeled DNA oligonucleotides: The uniformly ^{13}C , ^{15}N labeled A₆-DNA sample was prepared using chemically synthesized DNA (purchased from IDT), Klenow

fragment DNA polymerase (New England Biolab) and $^{13}\text{C}/^{15}\text{N}$ isotopically labeled dNTPs (Silantes) using the Zimmer and Crothers method (Zimmer and Crothers, 1995). The oligonucleotide was purified using 20 % 29:1 polyacrylamide denaturing gel with 8 M urea, 20 mM Tris borate and 1 mM EDTA, and then using electro-elution (Whatmann, GE Healthcare) in 40 mM Tris Acetate and 1 mM EDTA, followed by ethanol precipitation.

Sample annealing and buffer exchange: DNA/RNA oligonucleotides were re-suspended in water (200-500 μM). To prepare duplex samples, equimolar amounts of the constituent single stranded DNA/RNA samples were mixed and then heated at $T = 95^\circ\text{C}$ for ~5 min followed by cooling at room temperature for ~1 hour. All samples were exchanged three times into the desired buffer using centrifugal concentrators (4 mL, Millipore Sigma). 10 % D_2O (Millipore Sigma) was added to the samples prior to the NMR measurements.

Sample concentrations and buffer conditions: Unless mentioned otherwise, the NMR buffer contains 25 mM sodium chloride, 15 mM sodium phosphate, 0.1 mM EDTA and 10 % D_2O . Sample concentrations and buffer pH: $\text{A}_6\text{-DNA}$, 1.0 mM, pH 6.8; $\text{A}_2\text{-DNA}$, 1.0 mM, pH 5.4; $\text{A}_5\text{-DNA}$, 0.2 mM, pH 5.2; $\text{A}_6\text{-RNA}$, 0.5 mM, pH 6.8. Concentration was estimated by measuring the absorbance of the sample at

775 260nm and using extinction coefficients from the ADT Biol Oligo calculator
776 (<https://www.atdbio.com/tools/oligo-calculator>).
777

778 **4.2 NMR spectroscopy**

779 All NMR experiments were performed on a 600 BrukerAvance 3 spectrometer
780 equipped with a triple-resonance HCN cryo-genic probe. The NMR data were
781 processed and analyzed with NMRpipe (Delaglio et al., 1995) and SPARKY (T.D.
782 Goddard and D.G. Kneller, SPARKY 3, University of California, San Francisco).
783

784 *Resonance assignments:* Imino resonances were assigned using a combination
785 of 2D [¹H, ¹H] NOESY and [¹⁵N, ¹H] SOFAST-HMQC (Sathyamoorthy et al., 2014)
786 experiments. Assignments for A₆-DNA, A₂-DNA and A₆-RNA were reported
787 previously (Sathyamoorthy et al., 2017; Zhou et al., 2016; Nikolova et al., 2011).
788 The [¹H, ¹H] NOESY spectrum for A₅-DNA is shown in Fig. S1.
789

790 *¹H CEST:* The pulse sequence was shown in Fig. 1b, and was adapted from
791 Schlagnitweit *et al* (Schlagnitweit et al., 2018). [The q1 gradient \(Fig. 1b\) destroys](#)
792 [transverse ¹H magnetization prior to excitation of imino resonances. This helps to](#)
793 [avoid any accidental offset dependence of the starting ¹H magnetization.](#)

794 Relaxation delays $T_{EX} = 100$ ms was used for all ^1H CEST measurements at low
 795 temperatures ($5^\circ\text{C} - 30^\circ\text{C}$), while a shorter $T_{EX} = 80$ ms was used for high (45°C)
 796 temperature measurements. A longer $T_{EX} = 400$ ms was used to illustrate artefacts
 797 arising due to NOE dips (Fig. 3b). RF power and offset combinations used in the
 798 CEST measurements are given in Table S2. Calibration of RF field powers for the
 799 ^1H CEST measurements was performed as described previously (Rangadurai et
 800 al., 2019b) using the same pulse sequence. Field inhomogeneity was also
 801 measured (Fig. S10) using the same sequence and the procedure as described
 802 previously (Guenneugues et al., 1999). ^1H inhomogeneity was measured by
 803 performing on-resonance ^1H CEST experiments on G2-H1 of A_6 -DNA, chosen as
 804 it does not experience conformational exchange. The longest relaxation delay
 805 used for the measurements were 10 s, 2 s, 1 s, 0.4 s, 0.1 s and 0.04 s for RF fields
 806 10 Hz, 50 Hz, 100 Hz, 200 Hz, 1000 Hz and 4000 Hz, respectively. The resulting
 807 nutation curve was Fourier transformed and was fit to a gaussian function (blue
 808 lines in Fig. S10) to extract the full-width at half-maximum, which was used for
 809 defining the inhomogeneity as described previously (Guenneugues et al., 1999).
 810 The selective pulse was set to be off (Fig. 3b) by replacing pulse **a** (Fig. 1b) with a
 811 non-selective ^1H hard 90° pulse. 16 scans were used for A_6 -DNA (1.0 mM) at 5°C ,
 812 10°C , 20°C , 25°C , 30°C , and A_2 -DNA (1.0 mM) at 25°C . 32 scans were used for

[A₆-RNA \(0.5 mM\) at 25°C. 64 scans were used for A₅-DNA \(0.2 mM\) at 25°C and for A₆-DNA \(1.0 mM\) at 45°C.](#)

Fitting of ¹H CEST data: When performing 2-state CEST fitting with and without exchange, we restricted the offset to -6 to 6 ppm for ¹H CEST experiment with relaxation delay \leq 100 ms, and to -3 to 3 ppm for experiments with relaxation delay = 400 ms, to obviate any potential effects from ¹H-¹H cross-relaxation artifacts (Fig. 3b). Peak intensities of all imino protons in the 1D spectra as a function of RF power and offset frequency were extracted using NMRPipe (Delaglio et al., 1995). The peak intensity at a given RF power and offset is normalized by the average peak intensity over the triplicate CEST measurements with zero relaxation delay under the same RF power. The uncertainty in the measured peak intensity at each offset frequency and RF power combination was assumed to be equal to the standard deviation of the peak intensities for triplicate CEST experiments with zero relaxation delay under the same RF power (Zhao et al., 2014; Shi et al., 2019). CEST profiles were generated by plotting the normalized intensity as a function of offset $\Omega = \omega_{\text{RF}} - \omega_{\text{obs}}$ where ω_{obs} is the Larmor frequency of the observed resonance and ω_{RF} is the angular frequency of the applied RF field. RF field inhomogeneity (Fig. S10) was taken into account during CEST fitting as described previously (Rangadurai et al., 2020a). The normalized CEST profiles were then fit

via numerical integration of the Bloch-McConnell (B-M) equations as described previously (Rangadurai et al., 2020a). Fitting of CEST profiles without exchange (Fig. 4, Fig. S2-4) was performed by setting $p_{ES} = k_{ex} = \Delta\omega = 0$. Errors in exchange parameters were set to be equal to the fitting errors which were obtained as the square root of the diagonal elements of the covariance matrix. Reduced chi-square ($r\chi^2$) was calculated to assess the goodness of fitting (Rangadurai et al., 2019b). [Note that the variations in \$r\chi^2\$ values for different \$^1\text{H}\$ CEST profiles in Fig. 4 and Fig. S2-4 are most likely due to differences in the quality of the NMR data and poor estimation of the real experimental uncertainty.](#) The residual sum of squares (RSS) was computed as follows

$$RSS = \sum_{i=1}^n (I_i^{fit} - I_i^{exp})^2 \quad (1)$$

where I_i^{fit} and I_i^{exp} are the i th fit and experimentally measured intensity in the CEST profile respectively, and the summation is over all RF power and offset combinations (N).

Model selection for fits with and without exchange (Fig. 4, Fig. S2-4) was performed by computing AIC and BIC weights as follows (Burnham and Anderson, 2004):

$$AIC = \begin{cases} N \ln \left(\frac{RSS}{N} \right) + 2K, & \text{when } \frac{N}{K} \geq 40 \\ N \ln \left(\frac{RSS}{N} \right) + 2K + \frac{2K(K+1)}{N-K-1}, & \text{when } \frac{N}{K} < 40 \end{cases} \quad (2)$$

$$wAIC = \frac{e^{-0.5\Delta AIC}}{1 + e^{-0.5\Delta AIC}} \quad (3)$$

$$BIC = N \ln \left(\frac{RSS}{N} \right) + K \ln(N) \quad (4)$$

$$wBIC = \frac{e^{-0.5\Delta BIC}}{1 + e^{-0.5\Delta BIC}} \quad (5)$$

Where K is the number of floating parameters when fitting and $\Delta AIC/\Delta BIC$ are the differences between two AIC values (fitting without and with exchange). The AIC ($wAIC_{+ex}$) and BIC ($wBIC_{+ex}$) weights for fits with exchange are reported in Fig. 4 and Fig. S2-4. The improvement in the fit was considered statistically significant if both $wAIC_{+ex}$ and $wBIC_{+ex}$ values are > 0.995 , and $r\chi^2$ is reduced with the inclusion of exchange. For some resonances, the improvement in the fit with exchange are statistically significant but the resulting exchange parameters are not reliable and have large errors (see Fig. S2,3). For T4 in A5-DNA, $p_{ES} = 0.2 \pm 0.1$ % measured using 1H CEST was ~ 10 -fold smaller than $p_{ES} = 2.7 \pm 1.5$ % measured previously using ^{15}N RD (Alvey et al., 2014), whereas k_{ex} (~ 3000 s $^{-1}$) was in good agreement. However, simulations show that due to the small $\Delta\omega$ for ^{15}N (~ 1 ppm)

871 and fast exchange kinetics k_{ex} ($\sim 3000 \text{ s}^{-1}$) the p_{ES} and $\Delta\omega$ are not well-determined
872 by the ^{15}N RD data (Fig. S6c). For this reason, this data point was excluded for ^1H
873 CEST and $^{13}\text{C}/^{15}\text{N}$ RD comparison (Fig. 5a).

874

875 *Off-resonance ^{13}C $R_{1\rho}$ relaxation dispersion:* ^{13}C $R_{1\rho}$ experiments were performed
876 using 1D $R_{1\rho}$ schemes as described previously (Nikolova et al., 2012a; Nikolova
877 et al., 2011; Hansen et al., 2009). The spin-lock powers and offsets are listed in
878 Table S3. The spin-lock was applied for a maximal duration $< 60 \text{ ms}$ to achieve
879 $\sim 70 \%$ loss of peak intensity at the end of relaxation delay. Off-resonance $R_{1\rho}$
880 profiles (Fig. S8) were generated by plotting $(R_2 + R_{ex}) = (R_{1\rho} - R_1 \cos^2\theta)/\sin^2\theta$,
881 where θ is the angle between the effective field of the observed resonance and the
882 z-axis, as a function of $\Omega_{eff}/2\pi$, where $\Omega_{eff} = \omega_{obs} - \omega_{RF}$, where ω_{obs} is the Larmor
883 frequency of the spin and ω_{RF} is the carrier frequency of the applied spin-lock.

884

885 *Fitting of ^{13}C $R_{1\rho}$ data:* 1D peak intensities were measured using NMRpipe
886 (Delaglio et al., 1995). $R_{1\rho}$ values for a given spin-lock power and offset were
887 calculated by fitting the intensities as a function of delay time to a mono-
888 exponential decay (Kimsey et al., 2015). A Monte-Carlo approach was used to
889 calculate the uncertainties of $R_{1\rho}$ (Bothe et al., 2014). Alignment of initial
890 magnetization during the Bloch-McConnell fitting was performed based on the

891 $k_{\text{ex}}/\Delta\omega$ value (Rangadurai et al., 2019b). Chemical exchange parameters were
 892 obtained by fitting experimental $R_{1\rho}$ values to numerical solutions of a 2-state
 893 Bloch-McConnell (B-M) equations (McConnell, 1958). A Monte-Carlo approach
 894 was used to calculate the errors of exchange parameters (Bothe et al., 2014) .
 895 Reduced chi-square ($r\chi^2$) was calculated to assess the goodness of fitting
 896 (Rangadurai et al., 2019b).

897

898 **4.3 Thermodynamic Analysis**

899 The observed temperature dependence of k_1 , k_{-1} for the Watson-Crick to
 900 Hoogsteen exchange measuring using ^1H CEST were fit to a modified van't Hoff
 901 equation that accounts for statistical compensation effects and assumes a smooth
 902 energy surface as described previously (Nikolova et al., 2011; Coman and Russu,
 903 2005):

904

$$905 \quad \ln\left(\frac{k_i(T)}{T}\right) = \ln\left(\frac{k_B\kappa}{h}\right) - \frac{\Delta G_i^{\circ T}(T_{hm})}{RT_{hm}} - \frac{\Delta H_i^{\circ T}}{R} \left(\frac{1}{T} - \frac{1}{T_{hm}}\right) \quad (6)$$

906

907 k_i ($i = 1, -1$) is the forward and backward rate constants, $\Delta G_i^{\circ T}(T)$ and $\Delta H_i^{\circ T}$ are the
 908 free energy (at temperature T , in Kelvin) and enthalpy of activation ($i = 1$) or
 909 deactivation ($i = -1$) respectively. R is the universal gas constant ($\text{kcal mol}^{-1} \text{K}^{-1}$)

910 and T_{hm} is the harmonic mean of the experimental temperatures (T_i in K) computed
 911 as $T_{hm} = n / \sum_{i=1}^n (1/T_i)$, k_B is the Boltzmann's constant ($J K^{-1}$), κ is the
 912 transmission coefficient (assumed to be unity) and h is the Planck constant ($J s$).
 913
 914 The goodness-of-fit indicator R^2 (coefficient of determination) (Fig. S6) between
 915 the measured and fitted rate constants was calculated as follows: $R^2 = 1 -$
 916 $\frac{SS_{res}}{SS_{total}}$, $SS_{res} = \sum (k_{i,fit} - k_{i,exp})^2$, $SS_{total} = \sum (k_{i,exp} - \overline{k_{i,exp}})^2$. $k_{i,fit}$ and $k_{i,exp}$ (i
 917 = 1, -1) are fitted and experimentally measured rate constants. $\overline{k_{i,exp}}$ is the mean
 918 of all $k_{i,exp}$. Errors of fitting for $\Delta G_i^{\circ T}$ and ΔH_i^T were calculated as the square root
 919 of the diagonal elements of the covariance matrix. $T\Delta S_i^T$ is calculated as $\Delta H_i^T -$
 920 $\Delta G_i^{\circ T}$.

921 **Data and code availability.** The data that support this study are contained in the
922 published article (and its Supplementary Information) or are available from the
923 corresponding author on reasonable request. The python scripts for ^1H CEST data
924 fitting are available at <https://github.com/alhashimilab/1H-CEST>.

925

926 **Author contributions.** BL, AR, and HMA conceived the project and experimental
927 design. BL, AR, and HS prepared the samples and set up the imino ^1H CEST
928 experiment. BL performed ^1H CEST experiments and data analysis. HS
929 performed ^{13}C $R_{1\rho}$ experiments. HMA, BL, and AR wrote the manuscript with
930 critical input from HS.

931

932 **Competing interests.** The authors declare that they have no conflict of interest.

933

934 **Acknowledgments.** We thank Prof. Katja Petzold for sharing the ^1H CEST pulse
935 sequence. We thank Dr. Or Szekely for general input and Ainan Geng for help
936 with the ^1H inhomogeneity measurements.

937

938 **Financial Support.** This work was supported by the US National Institutes of
939 Health (R01GM089846) Grants to H.M.A.

Reference

- Afek, A., Shi, H., Rangadurai, A., Sahay, H., Senitzki, A., Xhani, S., Fang, M., Salinas, R., Mielko, Z., Pufall, M. A., Poon, G. M. K., Haran, T. E., Schumacher, M. A., Al-Hashimi, H. M., and Gordan, R.: DNA mismatches reveal conformational penalties in protein-DNA recognition, *Nature*, 587, 291-296, 10.1038/s41586-020-2843-2, 2020.
- Aishima, J., Gitti, R. K., Noah, J. E., Gan, H. H., Schlick, T., and Wolberger, C.: A Hoogsteen base pair embedded in undistorted B-DNA, *Nucleic acids research*, 30, 5244-5252, 2002.
- Alvey, H. S., Gottardo, F. L., Nikolova, E. N., and Al-Hashimi, H. M.: Widespread transient Hoogsteen base pairs in canonical duplex DNA with variable energetics, *Nat Commun*, 5, 4786, 10.1038/ncomms5786, 2014.
- Baronti, L., Guzzetti, I., Ebrahimi, P., Friebe Sandoz, S., Steiner, E., Schlagnitweit, J., Fromm, B., Silva, L., Fontana, C., Chen, A. A., and Petzold, K.: Base-pair conformational switch modulates miR-34a targeting of Sirt1 mRNA, *Nature*, 583, 139-144, 10.1038/s41586-020-2336-3, 2020.
- Ben Imeddourene, A., Zargarian, L., Buckle, M., Hartmann, B., and Mauffret, O.: Slow motions in A.T rich DNA sequence, *Sci Rep*, 10, 19005, 10.1038/s41598-020-75645-x, 2020.
- Bothe, J. R., Stein, Z. W., and Al-Hashimi, H. M.: Evaluating the uncertainty in exchange parameters determined from off-resonance R1rho relaxation dispersion for systems in fast exchange, *J Magn Reson*, 244, 18-29, 10.1016/j.jmr.2014.04.010, 2014.
- Bouvignies, G. and Kay, L. E.: Measurement of proton chemical shifts in invisible states of slowly exchanging protein systems by chemical exchange saturation transfer, *J Phys Chem B*, 116, 14311-14317, 10.1021/jp311109u, 2012.
- Burnham, K. P. and Anderson, D. R.: Multimodel inference - understanding AIC and BIC in model selection, *Sociol Method Res*, 33, 261-304, 10.1177/0049124104268644, 2004.
- Chen, B., LeBlanc, R., and Dayie, T. K.: SAM-II Riboswitch Samples at least Two Conformations in Solution in the Absence of Ligand: Implications for Recognition, *Angew Chem Int Edit*, 55, 2724-2727, 10.1002/anie.201509997, 2016.
- Coman, D. and Russu, I. M.: A nuclear magnetic resonance investigation of the energetics of basepair opening pathways in DNA, *Biophys J*, 89, 3285-3292, 10.1529/biophysj.105.065763, 2005.
- Czernek, J., Fiala, R., and Sklenar, V.: Hydrogen bonding effects on the (15)N and (1)H shielding tensors in nucleic acid base pairs, *J Magn Reson*, 145, 142-146, 10.1006/jmre.2000.2091, 2000.
- Delaglio, F., Grzesiek, S., Vuister, G. W., Zhu, G., Pfeifer, J., and Bax, A.: NMRPipe: a multidimensional spectral processing system based on UNIX pipes, *J Biomol NMR*, 6, 277-293, 10.1007/BF00197809, 1995.
- Dubini, R. C. A., Schon, A., Muller, M., Carell, T., and Rovo, P.: Impact of 5-formylcytosine on the melting kinetics of DNA by 1H NMR chemical exchange, *Nucleic Acids Res*, 48, 8796-8807, 10.1093/nar/gkaa589, 2020.
- Eichmuller, C. and Skrynnikov, N. R.: A new amide proton R1rho experiment permits accurate characterization of microsecond time-scale conformational exchange, *J Biomol NMR*, 32, 281-293,

979 10.1007/s10858-005-0658-y, 2005.
 980 Felsenfeld, G., Davies, D. R., and Rich, A.: Formation of a 3-Stranded Polynucleotide Molecule,
 981 Journal of the American Chemical Society, 79, 2023-2024, DOI 10.1021/ja01565a074, 1957.
 982 Frank, A. T., Horowitz, S., Andricioaei, I., and Al-Hashimi, H. M.: Utility of ^1H NMR chemical shifts
 983 in determining RNA structure and dynamics, J Phys Chem B, 117, 2045-2052, 10.1021/jp310863c,
 984 2013.
 985 Furukawa, A., Walinda, E., Arita, K., and Sugase, K.: Structural dynamics of double-stranded DNA
 986 with epigenome modification, Nucleic Acids Res, 49, 1152-1162, 10.1093/nar/gkaa1210, 2021.
 987 Golovenko, D., Brauning, B., Vyas, P., Haran, T. E., Rozenberg, H., and Shakked, Z.: New Insights
 988 into the Role of DNA Shape on Its Recognition by p53 Proteins, Structure, 26, 1237-1250 e1236,
 989 10.1016/j.str.2018.06.006, 2018.
 990 Guenneugues, M., Berthault, P., and Desvaux, H.: A method for determining B1 field inhomogeneity.
 991 Are the biases assumed in heteronuclear relaxation experiments usually underestimated?, J Magn
 992 Reson, 136, 118-126, 10.1006/jmre.1998.1590, 1999.
 993 Gueron, M. and Leroy, J. L.: Studies of base pair kinetics by NMR measurement of proton exchange,
 994 Methods Enzymol, 261, 383-413, 10.1016/s0076-6879(95)61018-9, 1995.
 995 Gueron, M., Kochoyan, M., and Leroy, J. L.: A single mode of DNA base-pair opening drives imino
 996 proton exchange, Nature, 328, 89-92, 10.1038/328089a0, 1987.
 997 Hansen, A. L., Lundstrom, P., Velyvis, A., and Kay, L. E.: Quantifying millisecond exchange
 998 dynamics in proteins by CPMG relaxation dispersion NMR using side-chain ^1H probes, J Am Chem
 999 Soc, 134, 3178-3189, 10.1021/ja210711v, 2012.
 1000 Hansen, A. L., Nikolova, E. N., Casiano-Negróni, A., and Al-Hashimi, H. M.: Extending the range of
 1001 microsecond-to-millisecond chemical exchange detected in labeled and unlabeled nucleic acids by
 1002 selective carbon R(1rho) NMR spectroscopy, J Am Chem Soc, 131, 3818-3819, 10.1021/ja8091399,
 1003 2009.
 1004 Hoogsteen, K.: The Structure of Crystals Containing a Hydrogen-Bonded Complex of 1-
 1005 Methylthymine and 9-Methyladenine, Acta Crystallogr, 12, 822-823, Doi
 1006 10.1107/S0365110x59002389, 1959.
 1007 Hwang, T. L. and Shaka, A. J.: Water Suppression That Works - Excitation Sculpting Using Arbitrary
 1008 Wave-Forms and Pulsed-Field Gradients, J Magn Reson Ser A, 112, 275-279, DOI
 1009 10.1006/jmra.1995.1047, 1995.
 1010 Ishima, R. and Torchia, D. A.: Extending the range of amide proton relaxation dispersion
 1011 experiments in proteins using a constant-time relaxation-compensated CPMG approach, J Biomol
 1012 NMR, 25, 243-248, 10.1023/a:1022851228405, 2003.
 1013 Ishima, R., Wingfield, P. T., Stahl, S. J., Kaufman, J. D., and Torchia, D. A.: Using amide H-1 and
 1014 N-15 transverse relaxation to detect millisecond time-scale motions in perdeuterated proteins:
 1015 Application to HIV-1 protease, Journal of the American Chemical Society, 120, 10534-10542, DOI
 1016 10.1021/ja981546c, 1998.
 1017 Juen, M. A., Wunderlich, C. H., Nussbaumer, F., Tollinger, M., Kontaxis, G., Konrat, R., Hansen, D.

1018 F., and Kreutz, C.: Excited States of Nucleic Acids Probed by Proton Relaxation Dispersion NMR
1019 Spectroscopy, *Angew Chem Int Ed Engl*, 55, 12008-12012, 10.1002/anie.201605870, 2016.

1020 Kimsey, I. J., Petzold, K., Sathyamoorthy, B., Stein, Z. W., and Al-Hashimi, H. M.: Visualizing
1021 transient Watson-Crick-like mispairs in DNA and RNA duplexes, *Nature*, 519, 315-320,
1022 10.1038/nature14227, 2015.

1023 Kimsey, I. J., Szymanski, E. S., Zahurancik, W. J., Shakya, A., Xue, Y., Chu, C. C., Sathyamoorthy,
1024 B., Suo, Z., and Al-Hashimi, H. M.: Dynamic basis for dG*dT misincorporation via tautomerization
1025 and ionization, *Nature*, 554, 195-201, 10.1038/nature25487, 2018.

1026 Kitayner, M., Rozenberg, H., Rohs, R., Suad, O., Rabinovich, D., Honig, B., and Shakked, Z.:
1027 Diversity in DNA recognition by p53 revealed by crystal structures with Hoogsteen base pairs, *Nat*
1028 *Struct Mol Biol*, 17, 423-429, 10.1038/nsmb.1800, 2010.

1029 Lam, S. L. and Chi, L. M.: Use of chemical shifts for structural studies of nucleic acids, *Prog Nucl*
1030 *Magn Reson Spectrosc*, 56, 289-310, 10.1016/j.pnmrs.2010.01.002, 2010.

1031 Lane, A. N., Bauer, C. J., and Frenkiel, T. A.: Determination of conformational transition rates in the
1032 trp promoter by ¹H NMR rotating-frame T1 and cross-relaxation rate measurements, *Eur Biophys*
1033 *J*, 21, 425-431, 10.1007/BF00185870, 1993.

1034 LeBlanc, R. M., Longhini, A. P., Tugarinov, V., and Dayie, T. K.: NMR probing of invisible excited
1035 states using selectively labeled RNAs, *J Biomol NMR*, 71, 165-172, 10.1007/s10858-018-0184-3,
1036 2018.

1037 Leijon, M. and Graslund, A.: Effects of sequence and length on imino proton exchange and base
1038 pair opening kinetics in DNA oligonucleotide duplexes, *Nucleic Acids Res*, 20, 5339-5343,
1039 10.1093/nar/20.20.5339, 1992.

1040 Leroy, J. L., Kochoyan, M., Huynh-Dinh, T., and Gueron, M.: Characterization of base-pair opening
1041 in deoxynucleotide duplexes using catalyzed exchange of the imino proton, *J Mol Biol*, 200, 223-
1042 238, 10.1016/0022-2836(88)90236-7, 1988.

1043 Ling, H., Boudsocq, F., Plosky, B. S., Woodgate, R., and Yang, W.: Replication of a cis-syn thymine
1044 dimer at atomic resolution, *Nature*, 424, 1083-1087, 10.1038/nature01919, 2003.

1045 Liu, B., Shi, H., Rangadurai, A., Nussbaumer, F., Chu, C. C., Erharter, K., Case, D. A., Kreutz, C.,
1046 and Al-Hashimi, H. M.: A quantitative model predicts how m6A reshapes the kinetic landscape of
1047 nucleic acid hybridization and conformational transitions, *bioRxiv*, 2020.

1048 Lu, L., Yi, C., Jian, X., Zheng, G., and He, C.: Structure determination of DNA methylation lesions
1049 N1-meA and N3-meC in duplex DNA using a cross-linked protein-DNA system, *Nucleic Acids Res*,
1050 38, 4415-4425, 10.1093/nar/gkq129, 2010.

1051 Lundstrom, P. and Akke, M.: Off-resonance rotating-frame amide proton spin relaxation
1052 experiments measuring microsecond chemical exchange in proteins, *J Biomol NMR*, 32, 163-173,
1053 10.1007/s10858-005-5027-3, 2005.

1054 Lundstrom, P., Hansen, D. F., Vallurupalli, P., and Kay, L. E.: Accurate measurement of alpha proton
1055 chemical shifts of excited protein states by relaxation dispersion NMR spectroscopy, *Journal of the*
1056 *American Chemical Society*, 131, 1915-1926, 10.1021/ja807796a, 2009.

1057 McConnell, H. M.: Reaction Rates by Nuclear Magnetic Resonance, *J Chem Phys*, 28, 430-431,
1058 Doi 10.1063/1.1744152, 1958.

1059 Nair, D. T., Johnson, R. E., Prakash, L., Prakash, S., and Aggarwal, A. K.: Hoogsteen base pair
1060 formation promotes synthesis opposite the 1,N6-ethenodeoxyadenosine lesion by human DNA
1061 polymerase α , *Nat Struct Mol Biol*, 13, 619-625, 10.1038/nsmb1118, 2006.

1062 Nikolova, E. N., Gottardo, F. L., and Al-Hashimi, H. M.: Probing transient Hoogsteen hydrogen
1063 bonds in canonical duplex DNA using NMR relaxation dispersion and single-atom substitution, *J*
1064 *Am Chem Soc*, 134, 3667-3670, 10.1021/ja2117816, 2012a.

1065 Nikolova, E. N., Bascom, G. D., Andricioaei, I., and Al-Hashimi, H. M.: Probing Sequence-Specific
1066 DNA Flexibility in A-Tracts and Pyrimidine-Purine Steps by Nuclear Magnetic Resonance C-13
1067 Relaxation and Molecular Dynamics Simulations, *Biochemistry*, 51, 8654-8664, 10.1021/bi3009517,
1068 2012b.

1069 Nikolova, E. N., Goh, G. B., Brooks, C. L., 3rd, and Al-Hashimi, H. M.: Characterizing the
1070 protonation state of cytosine in transient G.C Hoogsteen base pairs in duplex DNA, *J Am Chem*
1071 *Soc*, 135, 6766-6769, 10.1021/ja400994e, 2013a.

1072 Nikolova, E. N., Kim, E., Wise, A. A., O'Brien, P. J., Andricioaei, I., and Al-Hashimi, H. M.: Transient
1073 Hoogsteen base pairs in canonical duplex DNA, *Nature*, 470, 498-502, 10.1038/nature09775, 2011.

1074 Nikolova, E. N., Zhou, H., Gottardo, F. L., Alvey, H. S., Kimsey, I. J., and Al-Hashimi, H. M.: A
1075 historical account of Hoogsteen base-pairs in duplex DNA, *Biopolymers*, 99, 955-968,
1076 10.1002/bip.22334, 2013b.

1077 Otten, R., Villali, J., Kern, D., and Mulder, F. A.: Probing microsecond time scale dynamics in
1078 proteins by methyl (1)H Carr-Purcell-Meiboom-Gill relaxation dispersion NMR measurements.
1079 Application to activation of the signaling protein NtrC(r), *J Am Chem Soc*, 132, 17004-17014,
1080 10.1021/ja107410x, 2010.

1081 Palmer, A. G., 3rd: Chemical exchange in biomacromolecules: past, present, and future, *J Magn*
1082 *Reson*, 241, 3-17, 10.1016/j.jmr.2014.01.008, 2014.

1083 Rangadurai, A., Shi, H., and Al-Hashimi, H. M.: Extending the Sensitivity of CEST NMR
1084 Spectroscopy to Micro-to-Millisecond Dynamics in Nucleic Acids Using High-Power Radio-
1085 Frequency Fields, *Angew Chem Int Ed Engl*, 59, 11262-11266, 10.1002/anie.202000493, 2020a.

1086 Rangadurai, A., Kremser, J., Shi, H., Kreutz, C., and Al-Hashimi, H. M.: Direct evidence for
1087 (G)O6...H2-N4(C)(+) hydrogen bonding in transient G(syn)-C(+) and G(syn)-m(5)C(+) Hoogsteen
1088 base pairs in duplex DNA from cytosine amino nitrogen off-resonance R1rho relaxation dispersion
1089 measurements, *J Magn Reson*, 308, 106589, 10.1016/j.jmr.2019.106589, 2019a.

1090 Rangadurai, A., Szymanski, E. S., Kimsey, I. J., Shi, H., and Al-Hashimi, H. M.: Characterizing micro-
1091 to-millisecond chemical exchange in nucleic acids using off-resonance R1rho relaxation dispersion,
1092 *Prog Nucl Magn Reson Spectrosc*, 112-113, 55-102, 10.1016/j.pnmrs.2019.05.002, 2019b.

1093 Rangadurai, A., Shi, H., Xu, Y., Liu, B., Abou Assi, H., Zhou, H., Kimsey, I., and Al-Hashimi, H.:
1094 delta-Melt: Nucleic acid conformational penalties from melting experiments, *bioRxiv*, 2020b.

1095 Rangadurai, A., Zhou, H., Merriman, D. K., Meiser, N., Liu, B., Shi, H., Szymanski, E. S., and Al-

1096 Hashimi, H. M.: Why are Hoogsteen base pairs energetically disfavored in A-RNA compared to B-
 1097 DNA?, *Nucleic Acids Res*, 46, 11099-11114, 10.1093/nar/gky885, 2018.
 1098 Sathyamoorthy, B., Lee, J., Kimsey, I., Ganser, L. R., and Al-Hashimi, H.: Development and
 1099 application of aromatic [(13)C, (1)H] SOFAST-HMQC NMR experiment for nucleic acids, *J Biomol*
 1100 *NMR*, 60, 77-83, 10.1007/s10858-014-9856-9, 2014.
 1101 Sathyamoorthy, B., Shi, H., Zhou, H., Xue, Y., Rangadurai, A., Merriman, D. K., and Al-Hashimi, H.
 1102 M.: Insights into Watson-Crick/Hoogsteen breathing dynamics and damage repair from the solution
 1103 structure and dynamic ensemble of DNA duplexes containing m1A, *Nucleic Acids Res*, 45, 5586-
 1104 5601, 10.1093/nar/gkx186, 2017.
 1105 Schlagnitweit, J., Steiner, E., Karlsson, H., and Petzold, K.: Efficient Detection of Structure and
 1106 Dynamics in Unlabeled RNAs: The SELOPE Approach, *Chemistry*, 24, 6067-6070,
 1107 10.1002/chem.201800992, 2018.
 1108 Schnieders, R., Wolter, A. C., Richter, C., Wohner, J., Schwalbe, H., and Furtig, B.: Novel (13) C-
 1109 detected NMR Experiments for the Precise Detection of RNA Structure, *Angew Chem Int Ed Engl*,
 1110 58, 9140-9144, 10.1002/anie.201904057, 2019.
 1111 Sekhar, A., Rosenzweig, R., Bouvignies, G., and Kay, L. E.: Hsp70 biases the folding pathways of
 1112 client proteins, *Proc Natl Acad Sci U S A*, 113, E2794-2801, 10.1073/pnas.1601846113, 2016.
 1113 Shi, H., Clay, M. C., Rangadurai, A., Sathyamoorthy, B., Case, D. A., and Al-Hashimi, H. M.: Atomic
 1114 structures of excited state A-T Hoogsteen base pairs in duplex DNA by combining NMR relaxation
 1115 dispersion, mutagenesis, and chemical shift calculations, *J Biomol NMR*, 70, 229-244,
 1116 10.1007/s10858-018-0177-2, 2018.
 1117 Shi, H., Kimsey, I., Liu, H., Pham, U., Schumacher, M. A., and Al-Hashimi, H.: Revealing A-T and
 1118 G-C Hoogsteen base pairs in stressed protein-bound duplex DNA, *bioRxiv*, 2021.
 1119 Shi, H., Liu, B., Nussbaumer, F., Rangadurai, A., Kreutz, C., and Al-Hashimi, H. M.: NMR Chemical
 1120 Exchange Measurements Reveal That N(6)-Methyladenosine Slows RNA Annealing, *J Am Chem*
 1121 *Soc*, 141, 19988-19993, 10.1021/jacs.9b10939, 2019.
 1122 Singh, U. S., Moe, J. G., Reddy, G. R., Weisenseel, J. P., Marnett, L. J., and Stone, M. P.: 1H NMR
 1123 of an oligodeoxynucleotide containing a propanodeoxyguanosine adduct positioned in a (CG)3
 1124 frameshift hotspot of *Salmonella typhimurium* hisD3052: Hoogsteen base-pairing at pH 5.8, *Chem*
 1125 *Res Toxicol*, 6, 825-836, 10.1021/tx00036a012, 1993.
 1126 Smith, C. A., Ban, D., Pratihaar, S., Giller, K., Schwiegk, C., de Groot, B. L., Becker, S., Griesinger,
 1127 C., and Lee, D.: Population shuffling of protein conformations, *Angew Chem Int Ed Engl*, 54, 207-
 1128 210, 10.1002/anie.201408890, 2015.
 1129 Snoussi, K. and Leroy, J. L.: Imino proton exchange and base-pair kinetics in RNA duplexes,
 1130 *Biochemistry*, 40, 8898-8904, 10.1021/bi010385d, 2001.
 1131 Sipakdeevong, P., Cevec, M., Chang, A. T., Erat, M. C., Ziegeler, M., Zhao, Q., Fox, G. E., Gao,
 1132 X., Kennedy, S. D., Kierzek, R., Nikonowicz, E. P., Schwalbe, H., Sigel, R. K., Turner, D. H., and
 1133 Das, R.: Structure determination of noncanonical RNA motifs guided by (1)H NMR chemical shifts,
 1134 *Nature methods*, 11, 413-416, 10.1038/nmeth.2876, 2014.

1135 Steiner, E., Schlagnitweit, J., Lundstrom, P., and Petzold, K.: Capturing Excited States in the Fast-
 1136 Intermediate Exchange Limit in Biological Systems Using (HNMR)-H-1 Spectroscopy, *Angew*
 1137 *Chem Int Edit*, 55, 15869-15872, 10.1002/anie.201609102, 2016.
 1138 Stelling, A. L., Xu, Y., Zhou, H., Choi, S. H., Clay, M. C., Merriman, D. K., and Al-Hashimi, H. M.:
 1139 Robust IR-based detection of stable and fractionally populated G-C(+) and A-T Hoogsteen base
 1140 pairs in duplex DNA, *FEBS Lett*, 591, 1770-1784, 10.1002/1873-3468.12681, 2017.
 1141 Swails, J., Zhu, T., He, X., and Case, D. A.: AFNMR: automated fragmentation quantum mechanical
 1142 calculation of NMR chemical shifts for biomolecules, *Journal of biomolecular NMR*, 63, 125-139,
 1143 10.1007/s10858-015-9970-3, 2015.
 1144 Tateishi-Karimata, H., Nakano, M., and Sugimoto, N.: Comparable stability of Hoogsteen and
 1145 Watson-Crick base pairs in ionic liquid choline dihydrogen phosphate, *Sci Rep*, 4, 3593,
 1146 10.1038/srep03593, 2014.
 1147 Ughetto, G., Wang, A. H., Quigley, G. J., van der Marel, G. A., van Boom, J. H., and Rich, A.: A
 1148 comparison of the structure of echinomycin and triostin A complexed to a DNA fragment, *Nucleic*
 1149 *Acids Res*, 13, 2305-2323, 10.1093/nar/13.7.2305, 1985.
 1150 Wang, A. H., Ughetto, G., Quigley, G. J., Hakoshima, T., van der Marel, G. A., van Boom, J. H., and
 1151 Rich, A.: The molecular structure of a DNA-triostin A complex, *Science*, 225, 1115-1121,
 1152 10.1126/science.6474168, 1984.
 1153 Wang, S., Song, Y., Wang, Y., Li, X., Fu, B., Liu, Y., Wang, J., Wei, L., Tian, T., and Zhou, X.: The
 1154 m(6)A methylation perturbs the Hoogsteen pairing-guided incorporation of an oxidized nucleotide,
 1155 *Chem Sci*, 8, 6380-6388, 10.1039/c7sc02340e, 2017.
 1156 Wang, Y., Han, G., Jiang, X., Yuwen, T., and Xue, Y.: Chemical shift prediction of RNA imino groups:
 1157 application toward characterizing RNA excited states, *Nat Commun*, 12, 1595, 10.1038/s41467-
 1158 021-21840-x, 2021.
 1159 Wang, Y. S. and Ikuta, S.: Proton on-Resonance Rotating Frame Spin-Lattice Relaxation
 1160 Measurements of B and Z Double-Helical Oligodeoxyribonucleotides in Solution, *Journal of the*
 1161 *American Chemical Society*, 111, 1243-1248, DOI 10.1021/ja00186a013, 1989.
 1162 Weininger, U., Liu, Z., McIntyre, D. D., Vogel, H. J., and Akke, M.: Specific
 1163 ¹²Cβ₂D(2)¹²Cγ₂D(2)¹³S13Cε₁HD(2) isotopomer labeling of methionine to characterize
 1164 protein dynamics by ¹H and ¹³C NMR relaxation dispersion, *J Am Chem Soc*, 134, 18562-18565,
 1165 10.1021/ja309294u, 2012.
 1166 Weininger, U., Blissing, A. T., Hennig, J., Ahlner, A., Liu, Z., Vogel, H. J., Akke, M., and Lundstrom,
 1167 P.: Protein conformational exchange measured by ¹H R1ρ relaxation dispersion of methyl groups,
 1168 *J Biomol NMR*, 57, 47-55, 10.1007/s10858-013-9764-4, 2013.
 1169 Xu, Y., McSally, J., Andricioaei, I., and Al-Hashimi, H. M.: Modulation of Hoogsteen dynamics on
 1170 DNA recognition, *Nat Commun*, 9, 1473, 10.1038/s41467-018-03516-1, 2018.
 1171 Xu, Y., Manghrani, A., Liu, B., Shi, H., Pham, U., Liu, A., and Al-Hashimi, H. M.: Hoogsteen base
 1172 pairs increase the susceptibility of double-stranded DNA to cytotoxic damage, *J Biol Chem*, 295,
 1173 15933-15947, 10.1074/jbc.RA120.014530, 2020.

1174 Yamazaki, T., Muhandiram, R., and Kay, L. E.: NMR Experiments for the Measurement of Carbon
 1175 Relaxation Properties in Highly Enriched, Uniformly ^{13}C , ^{15}N -Labeled Proteins: Application to
 1176 ^{13}C .alpha. Carbons, *Journal of the American Chemical Society*, 116, 8266-8278,
 1177 10.1021/ja00097a037, 1994.
 1178 Yuwen, T., Sekhar, A., and Kay, L. E.: Separating Dipolar and Chemical Exchange Magnetization
 1179 Transfer Processes in (1) H-CEST, *Angew Chem Int Ed Engl*, 56, 6122-6125,
 1180 10.1002/anie.201610759, 2017a.
 1181 Yuwen, T. R., Huang, R., and Kay, L. E.: Probing slow timescale dynamics in proteins using methyl
 1182 H-1 CEST, *Journal of Biomolecular Nmr*, 68, 215-224, 10.1007/s10858-017-0121-x, 2017b.
 1183 Zhao, B., Hansen, A. L., and Zhang, Q.: Characterizing slow chemical exchange in nucleic acids
 1184 by carbon CEST and low spin-lock field R(1rho) NMR spectroscopy, *J Am Chem Soc*, 136, 20-23,
 1185 10.1021/ja409835y, 2014.
 1186 Zhou, H., Sathyamoorthy, B., Stelling, A., Xu, Y., Xue, Y., Pigli, Y. Z., Case, D. A., Rice, P. A., and
 1187 Al-Hashimi, H. M.: Characterizing Watson-Crick versus Hoogsteen Base Pairing in a DNA-Protein
 1188 Complex Using Nuclear Magnetic Resonance and Site-Specifically (^{13}C - and (^{15}N -Labeled DNA,
 1189 *Biochemistry*, 58, 1963-1974, 10.1021/acs.biochem.9b00027, 2019.
 1190 Zhou, H., Kimsey, I. J., Nikolova, E. N., Sathyamoorthy, B., Grazioli, G., McSally, J., Bai, T.,
 1191 Wunderlich, C. H., Kreutz, C., Andricioaei, I., and Al-Hashimi, H. M.: m(1)A and m(1)G disrupt A-
 1192 RNA structure through the intrinsic instability of Hoogsteen base pairs, *Nature structural &*
 1193 *molecular biology*, 23, 803-810, 10.1038/nsmb.3270, 2016.
 1194 Zimmer, D. P. and Crothers, D. M.: NMR of enzymatically synthesized uniformly ^{13}C ^{15}N -labeled
 1195 DNA oligonucleotides, *Proc Natl Acad Sci U S A*, 92, 3091-3095, 10.1073/pnas.92.8.3091, 1995.

1196